frontiers | Frontiers in Molecular Neuroscience

TYPE Original Research
PUBLISHED 26 February 2025
DOI 10.3389/fnmol.2025.1546375

OPEN ACCESS

EDITED BY
Dezhi Liao,
University of Minnesota Twin Cities,
United States

REVIEWED BY
Paulina Carriba,
Centre for Genomic Regulation (CRG), Spain
Erika Lorenzetto,
University of Verona, Italy

*CORRESPONDENCE
Stephen D. Ginsberg
✉ ginsberg@nki.rfmh.org

RECEIVED 16 December 2024
ACCEPTED 30 January 2025
PUBLISHED 26 February 2025

CITATION
Alldred MJ, Ibrahim KW, Pidikiti H, Lee SH, Heguy A, Chiosis G, Mufson EJ, Stutzmann GE and Ginsberg SD (2025) Profiling hippocampal neuronal populations reveals unique gene expression mosaics reflective of connectivity-based degeneration in the Ts65Dn mouse model of Down syndrome and Alzheimer's disease. *Front. Mol. Neurosci.* 18:1546375. doi: 10.3389/fnmol.2025.1546375

Profiling hippocampal neuronal populations reveals unique gene expression mosaics reflective of connectivity-based degeneration in the Ts65Dn mouse model of Down syndrome and Alzheimer's disease

Melissa J. Alldred[1,2], Kyrillos W. Ibrahim[1], Harshitha Pidikiti[1], Sang Han Lee[1,2], Adriana Heguy[3], Gabriela Chiosis[4,5], Elliott J. Mufson[6], Grace E. Stutzmann[7] and Stephen D. Ginsberg[1,2,8,9]*

[1]Center for Dementia Research, Nathan Kline Institute, Orangeburg, NY, United States, [2]Department of Psychiatry, New York University Grossman School of Medicine, New York, NY, United States, [3]Genome Technology Center, New York University Grossman School of Medicine, New York, NY, United States, [4]Program in Chemical Biology, Sloan Kettering Institute, New York, NY, United States, [5]Breast Cancer Medicine Service, Memorial Sloan Kettering Cancer Center, New York, NY, United States, [6]Department of Translational Neuroscience and Neurology, Barrow Neurological Institute, Phoenix, AZ, United States, [7]Center for Neurodegenerative Disease and Therapeutics, Rosalind Franklin University, The Chicago Medical School, North Chicago, IL, United States, [8]Department of Neuroscience and Physiology, New York University Grossman School of Medicine, New York, NY, United States, [9]NYU Neuroscience Institute, New York University Grossman School of Medicine, New York, NY, United States

Introduction: Individuals with Down syndrome (DS) exhibit neurological deficits throughout life including the development of in Alzheimer's disease (AD) pathology and cognitive impairment. At the cellular level, dysregulation in neuronal gene expression is observed in postmortem human brain and mouse models of DS/AD. To date, RNA-sequencing (RNA-seq) analysis of hippocampal neuronal gene expression including the characterization of discrete circuit-based connectivity in DS remains a major knowledge gap. We postulate that spatially characterized hippocampal neurons display unique gene expression patterns due, in part, to dysfunction of the integrity of intrinsic circuitry.

Methods: We combined laser capture microdissection to microisolate individual neuron populations with single population RNA-seq analysis to determine gene expression analysis of CA1 and CA3 pyramidal neurons and dentate gyrus granule cells located in the hippocampus, a region critical for learning, memory, and synaptic activity.

Results: The hippocampus exhibits age-dependent neurodegeneration beginning at ~6 months of age in the Ts65Dn mouse model of DS/AD. Each population of excitatory hippocampal neurons exhibited unique gene expression alterations in Ts65Dn mice. Bioinformatic inquiry revealed unique vulnerabilities and differences with mechanistic implications coinciding with onset of degeneration in this model of DS/AD.

Conclusions: These cell-type specific vulnerabilities may underlie degenerative endophenotypes suggesting precision medicine targeting of individual populations of neurons for rational therapeutic development.

KEYWORDS

Alzheimer's disease, bioinformatics, Down syndrome, hippocampus, laser capture microdissection, RNA sequencing, selective vulnerability, trisomy

Introduction

Down syndrome (DS), caused by the triplication of human chromosome 21 (HSA21), represents the most common genomic cause of intellectual disability with prevalence estimates of 1 in 700 live births in the United States (Mai et al., 2019; Parker et al., 2010). Individuals with DS have multiple neurodevelopmental phenotypes, mild to moderate intellectual impairment, neurological deficits, including reduced numbers and size of neurons in the hippocampus, along with systemic peripheral deficits (Rachidi and Lopes, 2008; Chapman and Hesketh, 2000; Lott, 2012; Wisniewski, 1990; Freeburn and Munn, 2021; Emili et al., 2024). DS results in memory deficits associated with impaired hippocampal function, including impairment in episodic and spatial memory (Freeburn and Munn, 2021; Chapman and Hesketh, 2000; Contestabile et al., 2017; Das et al., 2014). In addition, individuals with DS develop amyloid-beta peptide (Aβ) senile plaques, tau-containing neurofibrillary tangles, cortical thinning, and overt brain atrophy over their lifespan (Chapman and Hesketh, 2000; Mann et al., 1984; Lott and Head, 2019; Wisniewski et al., 1985). Most individuals with DS have documented progressive cognitive impairment, with dementia now described as the primary cause of death in adults with DS (Lott and Head, 2019; Landes et al., 2020).

Murine trisomic models of DS allow researchers to explore neuronal degenerative phenotypes at specific aging timepoints, linking them to the human condition. The Ts65Dn model is one of the oldest and most popular models of DS and AD (DS/AD) (Reeves et al., 1995; Davisson et al., 1993). Ts65Dn mice have a freely segregating mini-chromosome which encompasses a partial triplication of HSA21 orthologs on mouse chromosome 16 (Mmu16; ~90 protein-coding genes), along with a centromeric segment of non-orthologous mouse chromosome 17 (Mmu17; segment 17q1a) (Duchon et al., 2011; Sturgeon and Gardiner, 2011; Akeson et al., 2001). Ts65Dn mice recapitulate many of the endophenotypes associated with human DS, including early endosomal abnormalities (Cataldo et al., 2003; Cataldo et al., 2000), age-associated behavioral deficits in multiple domains of cognition (Powers et al., 2016; Hunter et al., 2003a; Hyde and Crnic, 2001; Fernandez and Garner, 2008), and frank neuronal loss (Gautier et al., 2023; Ash et al., 2014; Kelley et al., 2014b; Velazquez et al., 2013). Cognitive decline in DS has been associated with degeneration of the cholinergic septohippocampal pathway, arising from neuronal loss in the basal forebrain and loss of cholinergic fiber projection to the hippocampus and neocortex, which occurs in the Ts65Dn model of DS/AD (Perez et al., 2019; Velazquez et al., 2013; Powers et al., 2016; Peng et al., 2009; Kelley et al., 2014b; Hamlett et al., 2016; Gautier et al., 2023; Strupp et al., 2016). Moreover, Ts65Dn mice display reduced hippocampal neurogenesis (Bianchi et al., 2010; Velazquez et al., 2013; Insausti et al., 1998), hippocampal synapse loss (Kurt et al., 2004; Popov et al., 2011), and synaptic structural abnormalities (Belichenko et al., 2007; Belichenko et al., 2004; Kleschevnikov et al., 2012a). Degeneration of the cholinergic septohippocampal circuit, a cardinal feature of DS and AD (Granholm et al., 2000; Whitehouse et al., 1982; Yates et al., 1980), starts at approximately 6 months of age (MO) in the Ts65Dn mouse model (Rueda et al., 2012; Gotti et al., 2011; Holtzman et al., 1996). However, the underlying cellular mechanisms driving degeneration of this circuit are understudied.

Previous hippocampal analysis of synaptic structural and functional alterations in DS have linked impaired plasticity as a causal agent of cognitive decline (Kleschevnikov et al., 2004; Costa and Grybko, 2005; Kurt et al., 2004). Ts65Dn mice display decreased excitatory neurons and synaptic density (Kurt et al., 2004), and increased inhibitory neurons and synapses in the hippocampus (Chakrabarti et al., 2010; Belichenko et al., 2004). In the CA1 sector of the hippocampus, decreased long-term potentiation (LTP) occurs at 2 MO and 9 MO in Ts65Dn mice (Siarey et al., 1997), while field potential recordings centered in the CA1 region showed increased long-term depression (LTD) in 2MO Ts65Dn mice (Siarey et al., 1999). Increased spontaneous inhibitory postsynaptic current frequency was observed independently in the Ts65Dn CA1 sector, but no difference was observed in miniature IPSCs (mIPSCs) (Chakrabarti et al., 2010). In contrast, neurons in the Ts65Dn CA3 sector of the hippocampus have decreased mIPSCs and miniature excitatory postsynaptic currents (Hanson et al., 2007; Stagni et al., 2013; Contestabile et al., 2017). Electrophysiological analysis of dentate gyrus granule cells (DGCs) revealed increased inhibitory currents and synaptic density along with decreased LTP (Contestabile et al., 2017; Kleschevnikov et al., 2012b; Kleschevnikov et al., 2004; Contestabile et al., 2013). Taken together, these electrophysiological studies confirm an imbalance of excitation and inhibition in the hippocampus, postulated to be causal to the spatial and episodic memory impairments in DS mouse models, substantiated by GABA and NMDA receptor pharmacotherapies (Fernandez et al., 2007; Costa, 2011; Costa et al., 2008). However, most of these studies were performed in juvenile pups, prior to onset of septohippocampal degeneration, with virtually no assessment of the effects of aging on this learning and memory circuit.

Recent RNA sequencing (RNA-seq) analysis of neurons within medial septal nucleus (MSN) by our laboratory revealed transcriptomic alterations in Ts65Dn mice at the start (~6 MO) of basal forebrain cholinergic neuron (BFCN) degeneration (Alldred et al., 2021c; Alldred et al., 2023). However, hippocampal gene expression studies in postmortem human DS and DS/AD mouse models have mostly been limited to microarray and RT-qPCR based analyses (Alldred et al., 2018; Alldred et al., 2015a; Alldred et al., 2015b; Ahmed et al., 2012; Bofill-De Ros et al., 2015; Granholm et al., 2003; Hunter et al., 2003b; Pollonini et al., 2008). Although a few RNA-seq studies have been performed, most examined the entire hippocampus (Zhou et al., 2023; Granno et al., 2019; Hu et al., 2022), with limited assessment of individual hippocampal subregions in DS/AD models (Alldred et al., 2024a; Sierra et al., 2024). Both our study of laser capture microdissection (LCM) microisolated CA1 pyramidal neurons in ~11 MO female DS mice using the Ts2 derivative of the Ts65Dn model and the single nucleus RNA-seq performed on multiple hippocampal neuronal subtypes exhibited fewer dysregulated genes and pathways compared to the 6 MO MSN BFCNs (Alldred et al., 2024a; Sierra et al., 2024), leading to the hypothesis that (*i*) hippocampal neuronal degeneration lags behind that seen in basal forebrain and/or (*ii*) BFCNs degeneration precedes or paces hippocampal

degeneration in the context of DS/AD (Alldred et al., 2023; Alldred et al., 2021c; Mufson et al., 2021).

To evaluate hippocampal neuronal populations, we performed single population gene expression analysis to interrogate CA1 and CA3 pyramidal neurons (PNs) and DGCs. Samples were microisolated by LCM in the same spatial plane, followed by RNA-seq and downstream bioinformatic inquiry to analyze differentially expressed genes (DEGs) and pathway alterations in spatially characterized hippocampal excitatory neuronal populations in the Ts65Dn mice compared to normal disomic (2N) controls at 6 MO. We postulate each excitatory neuron population will display unique gene expression, with a subset of DEGs showing convergent dysregulation in all three populations.

Materials and methods

Mice

Ts65Dn (Ts, $n = 6$) and disomic (2N, $n = 6$) male mice (age range: 5.7–6.4 MO, mean age 6.0 MO) were generated as part of previously published studies by our group (Alldred et al., 2023; Alldred et al., 2021c).

Tissue accession

Brains were accessed as previously described (Alldred et al., 2021c, 2023). Following removal of the brain from the calvarium, a biased hemibrain dissection was performed, isolating one hemisphere ~1–1.5 mm lateral to the midline to preserve centrally located structures, including the basal forebrain nuclei, which was utilized in the previous studies (Alldred et al., 2021c; Alldred et al., 2023). This hemibrain containing the midline structures was flash frozen on dry ice for RNA-seq analysis. Sections of rostral hippocampus were cut on a cryostat (−25°C; CM1860UV, Leica, Buffalo Grove, IL) at a thickness of 20 µm and mounted on polyethylene naphthalate membrane slides (Leica) (Alldred et al., 2024a; Alldred and Ginsberg, 2023; Alldred et al., 2023; Alldred et al., 2021c). Slides were immediately stored under desiccant at-80°C until used for LCM. The other hemisphere (minus the midline structures) from the same mice utilized for RNA-seq was isolated and dissected for a CA1 enriched dissection and a CA3 + DG sector enrichment (Ts, $n = 6$; 2N, $n = 6$). In one 2N case, the other hemisphere was not available, so a 2N littermate was used for protein dissection. Briefly, an ~1.5 mm thick coronal slab was cut from the rostral hippocampus and placed on a dissection microscope (Zeiss Axiosplat). Under magnification (32x), a CA1 sector enriched dissection was isolated from the rest of the hippocampus with the resulting rest of the hippocampus termed CA3 sector + DG enrichment. Each dissected piece was flash frozen on dry ice and stored at-80°C. RNase-free precautions were employed, and solutions were made with 18.2 mega Ohm RNase-free water (Nanopure Diamond, Barnstead, Dubuque, IA).

Neuron collection

Polyethylene naphthalate membrane slides containing the rostral hippocampus were equilibrated to room temperature (RT) under desiccant (−20°C for 5 min, 4°C for 10 min, RT for 5 min) followed by a rapid Nissl staining protocol as previously described to preserve intact RNA in unfixed tissue (Alldred and Ginsberg, 2023). CA1 and CA3 PNs along with DGCs were identified visually in the same section and microisolated using the draw and cut feature by LCM for each section (LMD7000; Leica; Figures 1A,B). As the excitatory neurons are densely packed in these regions, groups of neurons were collected during LCM, with an estimated number of neurons per area collected. Approximately 6 rostral hippocampal tissue sections were dissected via LCM (approximately -1.58 to -2.54 Bregma), with mean collections of ~950 CA1 PNs, ~750 CA3 PNs, and ~ 1,175 DGCs per brain before proceeding to RNA isolation and RNA-seq library preparation.

RNA purification

RNA from neurons collected for each brain region (CA1, CA3, and DG) was purified using the miRNeasy Micro kit (Qiagen) according to manufacturers' specifications, which isolates total RNA including microRNAs. A DNase digestion was performed twice sequentially before the final washes and RNA purification. RNA quality control (QC) was performed (High Sensitivity RNA assay, Tapestation, Agilent, Santa Clara, CA). RNA Integrity Number (RIN) values ranged from 5.0–8.2 for all samples quantified, with samples at the limit of resolution measured by DV_{200} values.

Library preparation and RNA-seq

The SMARTer Stranded Total RNA-Seq kit-Pico input Mammalian v3 (Takara Bio, Mountain View, CA) was employed with unique indexes for each sample. To normalize input, CA1, CA3 and DG RNA concentrations were used to determine sample input, with an average of ~3–3.75 ng RNA input utilized per sample. Samples were fragmented for 3.75 min, with 5 cycles for PCR1 and 14 cycles for PCR2. Samples were quantified (Tapestation D1000 DNA assay; Agilent). One 2N sample for CA1 failed QC for library preparation, so neurons from all three regions (CA1, CA3, and DG) were re-isolated using adjacent tissue sections from the same mouse. LCM, RNA extraction and library preparation were performed and the sample passed QC. Samples were pooled in equimolar concentrations and assayed on a NovaSeq 6000 (Illumina, San Diego, CA) using an S1 100 cycle flow cell (v1.5) by the New York University Grossman School of Medicine Genome Technology Center.

RNA-seq processing

FastQ files were utilized for both conditions (Ts and 2N) in all three cell types (CA1 PNs, CA3 PNs, DGCs) to analyze data in parallel. FastQ files were generated and QC of the raw reads was performed by FastQC v0.11.9 (Andrews, 2010). Samples were removed from analysis if sequence counts were low (<100 k bases). One CA1 PN Ts sample was removed (<75 aligned reads). Read trimming was then performed as necessary by Trimmomatic 0.39 (Bolger et al., 2014). If QC passed and showed no adapter contamination, this step was skipped. Sequence reads were indexed and aligned to the reference genome (Gencode GRCm39-mm39)

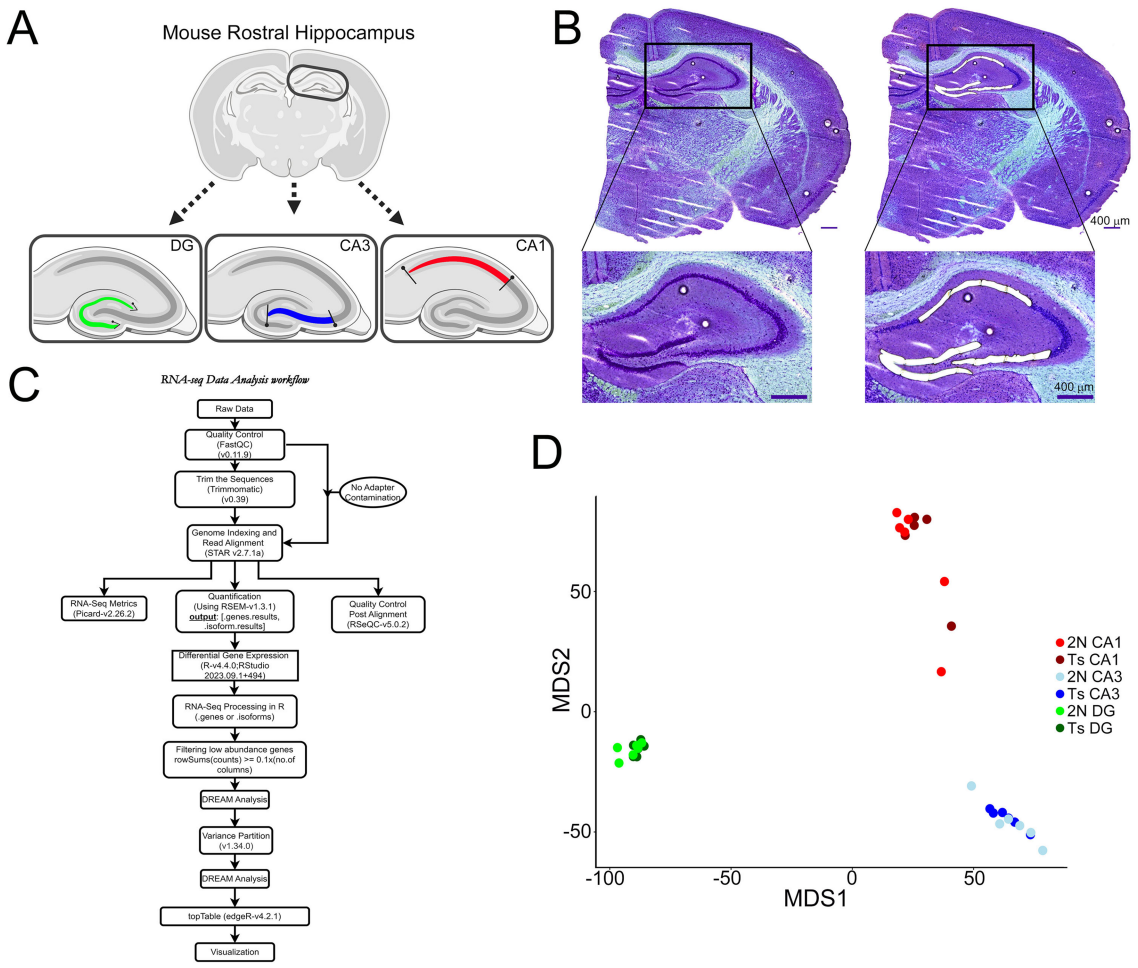

FIGURE 1
Microisolation and RNA-seq workflow for CA1 PNs, CA3 PNs, and DGCs. **(A)** Schematic representation indicates LCM paradigm to collect excitatory neurons from each hippocampal subregion in a single coronal section (schematic generated via BioRender). **(B)** A representative image shows a coronal section Nissl-stained section at 5x prior to (left) and after (right) microisolation of CA1 PNs, CA3 PNs, and DGCs, with insets showing higher resolution of tightly packed neurons acquired via LCM. Scale bar = 400 µm. **(C)** Overview of the single population RNA-seq bioinformatics analysis paradigm (generated in Drawio). **(D)** MDS plots use a colored dot to represent each individual sample for CA1 PNs (2N = light red; Ts = dark red), CA3 PNs (2N = light blue; Ts = dark blue) and DGCs (2N = light green; Ts = dark green).

using STAR Aligner (2.7.1a) (Dobin et al., 2013). Quantification was performed on alignments using Picard 2.26.2 (Picard Toolkit, 2019) for different measures and RSEM (1.3.1) for output (Li and Dewey, 2011). QC was performed on alignments using RSeQC (v5.0.2) (Wang et al., 2012). Differential gene expression was performed using R version4.4.0/RStudio v1 + 494 using genes results with the mouse reference genome (Gencode GRCm39-mm39) (Figure 1C; Supplementary Figure S1).

Statistical analysis

Gene Count matrix obtained from RSEM was analyzed. Genes with over 0.1 counts per million for at least 10 samples were retained, TMM normalization was then implemented by edgeR (Robinson et al., 2010) for downstream analysis. This step removes lowly expressed genes as they provide little evidence of differential expression and increase statistical errors and false discovery rate (Zehetmayer et al., 2022; Rau et al., 2013; Robinson et al., 2010). Analyses were performed using the DREAM pipeline (Hoffman and Roussos, 2021) which is built using the limma-voom framework from the VariancePartition (v.1.34.0) package (Hoffman and Schadt, 2016). In addition to Group and RNA concentration, the following variables were included as covariates: Intergenic percentage, Intronic percentage, mRNA base percentage, Usable base percentage, and Correct strand reads percentage. The covariates were computed from RNA-seq reads by Picard, with the exception of Group and RNA concentration. Multidimensional Scaling (MDS) was used to visualize the distribution of points and if necessary, identify the presence of outliers. Rrcov was utilized in R to detect the presence of outliers (Filzmoser and Todorov, 2013; Todorov, 2024). No outliers were detected or removed. TopTable (edgeR; v4.2.1) extracts genes that are present for all comparisons. Gene expression differences at ($p < 0.05$) were considered statistically significant. Protein coding genes were extracted using the R Bioconductor package AnnotationDbi (Pages et al., 2019). Multiple testing corrections were performed by false discovery rate (Broberg, 2005; Figure 1C). To ensure isolated cells were excitatory PNs and GCs, statistical analysis was performed in R

using the lmer package to normalized cell counts whereupon excitatory neuronal markers were compared to all other cell specific markers (Mathys et al., 2023) modeled as a function of group (Ts versus 2N) as previously described (Supplementary Figures S2A–C; Alldred et al., 2024b, Alldred et al., 2024a). Significance was judged at the level $\alpha = 0.05$, two-sided.

Pathway analyses

Pathway analyses consisted of Ingenuity Pathway Analysis (IPA; Qiagen) (Qiagen, 2020; Krämer et al., 2013), Gene Ontology (GO) (Ashburner et al., 2000; Gene Ontology Consortium, 2021) and STRING (Szklarczyk et al., 2018) in Cytoscape (cutoff 0.4) (Shannon et al., 2003). Shiny package (v.1.8.1.1) was utilized to create a web-based app to run GO analysis using R version 4.4.0/ RStudio v1 + 494. This app was also used to filter keyword targets to identify classes of processes affected by genotype and region (Alldred et al., 2024b; Alldred et al., 2024a; Alldred et al., 2023). Overlapping and unique processes were identified using Excel for IPA canonical pathways and neurological diseases and functions (D/Fs), along with GO processes. IPA gene network plots were generated using Igraph (v.2.0.3). STRING analysis was performed (Ts compared to 2N) separately for CA1 PNs, CA3 PNs, and DGCs DEGs to isolate top protein–protein interactions (PPIs) differentially expressed in Ts mice for each cell type. Venn diagrams were generated using InteractiVenn program (Heberle et al., 2015).

Protein analysis

For protein homogenization, all steps were performed on wet ice or at 4°C. Regional dissections of the hippocampus were utilized to generate the nanogram quantities needed for WES protein analysis (Alldred et al., 2024b; Alldred et al., 2021a; Alldred et al., 2021b). This is technically impractical by LCM (Alldred et al., 2024b; Alldred and Ginsberg, 2023). Each sample received 50 µL of tissue homogenization buffer (THB; 250 mM sucrose, 20 mM Tris base,1 mM EDTA, and 1 mM EGTA) with 1/100 volume of 100 mM phenylmethylsulfonyl fluoride (PMSF; Sigma, P7626) and 1/1000 volume of a protease inhibitor cocktail (Sigma; I3786) as described previously (Alldred et al., 2024b, Alldred et al., 2021a, Alldred et al., 2021b). Manual homogenization using a disposable microfuge pestle was performed for each sample in the microfuge tube, followed by a 5 min centrifugation step at 300 x g to pellet cell debris. The supernatant was extracted to a fresh microfuge tube and stored on wet ice while quantification was performed by the Bradford assay (23236; Coomassie Plus, ThermoFisher, Waltham, MA,) on a Nanodrop 2000C (ThermoFisher). The assay was performed per manufacturer's specifications with alterations to reduce volume, using bovine serum albumin to generate a standard curve (2 µL protein +58 µL reagent). Once quantification was performed, each sample was diluted to 2 mg/ml concentration using ice-cold THB with protease inhibitors, aliquoted and stored at-20°C until used for protein analysis.

Protein analysis was performed using the WES system (Protein Simple, San Jose, CA). Briefly, 3 µL of each sample was aliquoted to an individual well with 0.8 µL of 5x Fluorescent Master mix following WES protocol guidelines (Alldred et al., 2021a; Alldred et al., 2021b; Alldred et al., 2024b) using the 25 capillary 12–240 kD Wes separation module, to include all 24 samples ($n = 6$/genotype/region) and molecular mass ladder. Blocking reagents, primary and secondary antibodies, chemiluminescent substrate, separation and stacking matrices (Protein Simple) were dispensed to designated wells per manufacturer guidelines. Primary antibodies included mouse anti-β-tubulin III (β-TUBIII) used as input control (MAB1195, 1:50, R&D Systems, Minneapolis, MN), amyloid precursor protein (APP; C1/6.1, 1:20, gift of Dr. P.M. Mathews), which recognizes both full length APP as well as the β-CTF fragment (Mathews et al., 2002) and dual specificity tyrosine phosphorylation regulated kinase 1a (DYRK1A; D30C10 #8765, 1:20, Cell Signaling, Danvers, MA). Plates were spun for 5 min at 1000 x g and loaded onto a WES unit, where separation electrophoresis and immunodetection steps are fully automated within the capillary system. Instrument default settings were used with an increased run time to 35 min from default 25 min. Digital images were analyzed with Compass software (Protein Simple), utilizing dropped lines for peak analysis area calculation. Detected proteins were compared to control β-TUBIII levels and reported as normalized percentage of 2N CA1 sector mean. Each protein was performed in triplicate on separate plate runs. Statistical analysis was conducted on each protein compared to β-TUBIII and normalized to 2N CA1 sector mean to standardize means across assay runs. Samples were modeled as a function of the hippocampal region and genotype.

Results

Herein, we illustrate genotype differences are cell specific in the hippocampus during onset of BFCN degeneration utilizing LCM to isolate three distinct cell types within the hippocampal formation and analyzing gene expression. Using male Ts and 2N mice at the start of BFCN degeneration (~6 MO), CA1 PNs and CA3 PNs, along with DGCs from the rostral hippocampus were identified (Figure 1A) and isolated by LCM (Figure 1B). RNA-seq was performed with subsequent bioinformatic inquiry using the DREAM pipeline in which genotype and cell type differences were identified in Ts versus 2N mice, as seen by voom:mean–variance trend plots using a retention threshold of 10 for all three neuronal populations (Figure 1C; Supplementary Figures S1A–C).

Hippocampal genotype and cell specific differential gene expression in Ts mice

MDS analysis revealed distinct profiles for CA1 PNs, CA3 PNs, and DGCs (Figure 1D), with less robust differences seen in Ts versus 2N comparisons for all hippocampal neuron populations (Figure 1D; Supplementary Figures S1D–F), paralleling the Uniform Manifold Approximation and Projection (UMAP) analysis demonstrated previously in trisomic mice (Sierra et al., 2024). DEGs ($p < 0.05$) were identified for CA1 PNs, CA3 PNs, and DGCs by genotype (Ts versus 2N), with fewer genotype differences at 6 MO compared to the cell type differences. Interestingly, CA3 PNs had the most DEGs (1,566, Supplementary Table S2), more than CA1 PNs (947 DEGs; Supplementary Table S1) and DGCs (692 DEGs; Supplementary Table S3). Volcano plots show downregulated ($p < 0.05$, light blue; $p < 0.01$, dark blue) and upregulated ($p < 0.05$,

red; $p < 0.01$, dark red) DEGs sorted by log-fold change (LFC; base 2) and −log(p-value) for CA1 PNs (Figure 2A), CA3 PNs (Figure 2B), and DGCs (Figure 2C). Bar charts were utilized to bin genes by 0.25 increments of the LFC. CA1 PNs (Figure 2D) exhibited more upregulated (508) compared to downregulated (439) DEGs, while CA3 PNs (Figure 2E) and DGCs (Figure 2F) had approximately equal numbers of upregulated and downregulated DEGs. This suggests gene expression defects extend beyond the triplicated region within trisomic hippocampal neurons, with CA3 PNs neurons exhibiting the most robust dysregulation at 6 MO.

To ensure the number of DEGs isolated was not caused by overt differences in total number of genes analyzed that passed QC, the percentage of DEGs compared to genes analyzed was identified. While CA3 PNs had the highest total number of genes pass QC, DGCs also had a higher total number pass QC compared to CA1 PNs. However, DGCs had the lowest percentage of DEGs compared to analyzed genes (5.78%), followed by CA1 PNs (8.32%), with CA3 PNs having the highest ratio of DEGs compared to analyzed genes (12.82%; Figure 3A). This suggests that a higher number of genes passing QC may improve statistical analysis of DEGs, but at best, it only partially affects the total DEG outcome.

DEGs for each neuronal population were compared for genotype and circuitry effects, as indicated by convergent and unique gene expression. In each neuronal population, the vast majority of DEGs were unique to each neuronal population (Figure 3B), reinforcing each cell type has a unique expression profile. A total of 38 DEGs were found to be dysregulated in all three excitatory hippocampal populations, with 31 convergently dysregulated. CA1 PNs and CA3 PNs had more overlap of genotype dependent gene expression alterations with 90 total convergent DEGs (Figure 3B). CA1 PNs and DGCs had the least overlap, suggesting genotype dependent changes are highly specialized to cell type, while CA3 PNs and DGCs had the highest number of DEGs expressed in both neuronal populations (Figure 3B). This indicates that CA3 and DG neuronal clusters may have more convergent mechanisms of action which requires evaluation through IPA and GO analysis.

To examine PPIs using DEGs for each neuronal population, STRING in Cytoscape was performed on all DEGs for each region. CA1 PNs had 890 identified protein coding DEGs (of the 947 DEGs), which showed 3,819 total PPIs (Supplementary Figure S3A). These PPIs were then re-examined for the top interactors. STRING was performed on the top 40 PPIs in CA1 PNs with a minimum of 29 PPI partners and indicated a highly interactive PPI network (Figure 3C). CA3 DEGs were examined with 1,482 DEGs identified in STRING, which showed 7,634 total PPIs (Supplementary Figure S3B). The top 38 PPIs with 41 or more PPI partners, showed a closely interacting PPI network, with a highly concentrated cluster of PPI partners at the center of the network (Figure 3D). DGC significant genes (658 protein coding DEGs) showed the fewest interactions (1,705; Supplementary Figure S3C). Interestingly, when the top DEGs were examined in STRING (38 DEGs with 16+ PPI partners), there was a subset of 5 DEGs distinct from the majority of the PPI network

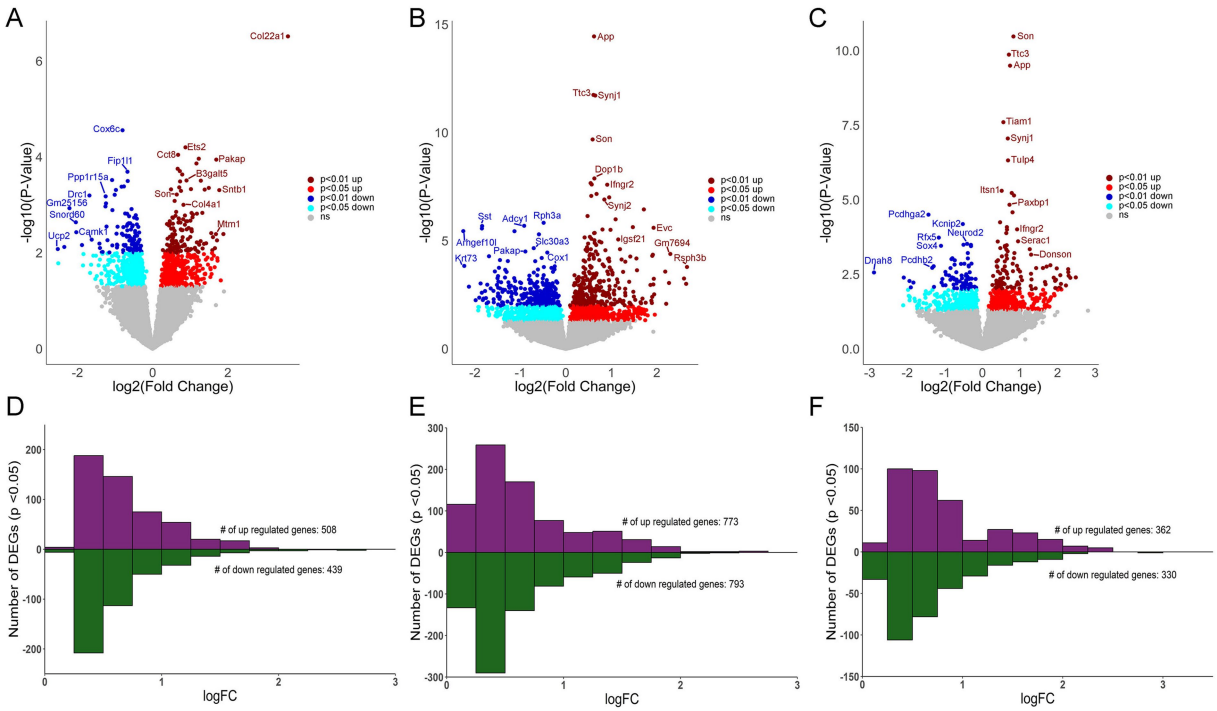

FIGURE 2
Differential gene expression in CA1 PNs, CA3 PNs and DGCs. **(A)** Volcano plot shows CA1 PN DEGs by genotype with LFC on the x-axis and significance [−log (p-value)] on the y-axis. **(B)** DEGs are both upregulated and downregulated as in a volcano plot in CA3 PNs by genotype. **(C)** Volcano plot depicting DEGs in DGCs by genotype. Key: Dark red dots ($p < 0.01$ upregulated), light red ($p < 0.05$ upregulated), dark blue ($p < 0.01$ downregulated) and light blue ($p < 0.05$ downregulated), with non-significant genes shown in grey. **(D–F)** Bar charts represent upregulated and downregulated DEGs by LFC (binned by 0.25 increments), with the majority of CA1 **(D)**, CA3 **(E)**, and DG **(F)** DEGs displaying <1 LFC difference by genotype (Ts versus 2N).

10.3389/fnmol.2025.1546375

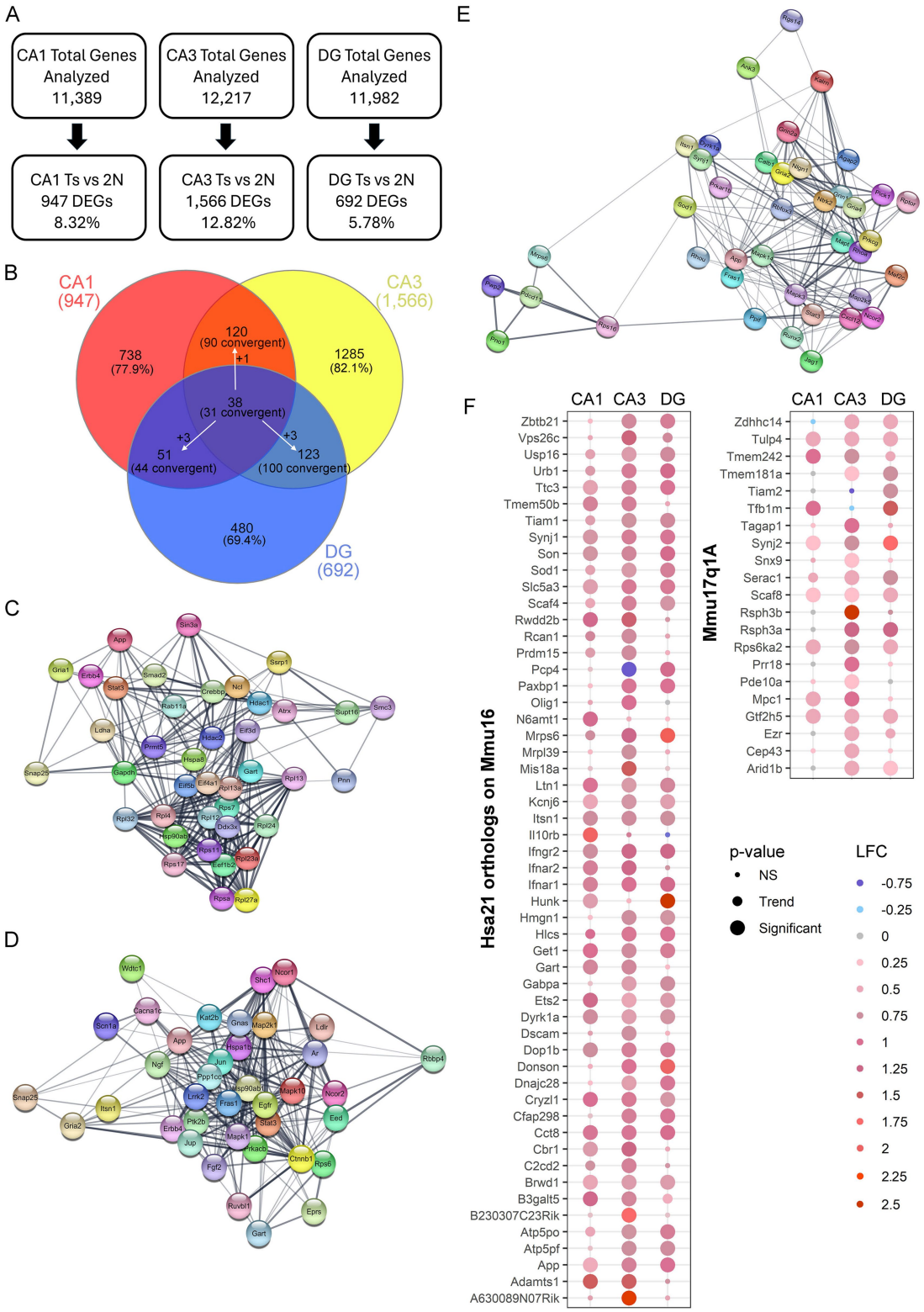

FIGURE 3
Hippocampal gene expression analysis in excitatory neuron populations. **(A)** Genes passing QC had <10% difference in total expression. Number and/or percentage of DEGs varied by hippocampal neuronal population. **(B)** Venn diagram of DEGs comparing each neuronal population indicated only a few DEGs overlap between CA1 PNs, CA3 PNs, and DGCs. White arrows indicate a DEG was dysregulated uniquely in one population, but convergently dysregulated in the other two. **(C)** STRING plots show the top 40 PPI with at least 29 total PPIs in CA1 PN DEGs, which are presented with each node having a DEG, with edges connecting the interaction partners. **(D)** Plot represents STRING analysis of the top 38 PPI interactors in CA3 PN DEGs which all had at least 41 total PPIs. **(E)** STRING analysis in DGCs showed the top 40 PPIs with overall fewer total PPI partners (>15 partners). STRING plot indicates these PPIs as two unique networks connected by two ribosomal DEGs. **(F)** Dot plots show triplicated DEGs that are HSA21 orthologs (left) or non-orthologous triplicated DEGs from the 17q1a fragment in the Ts mice (right) were identified by *p*-value (size) and LFC (color) with downregulation in shades of blue and upregulation in shades of red.

(Figure 3E). Only amyloid precursor protein (*App*) is convergently upregulated in all three networks. The paucity of convergent top PPIs in the excitatory neuron hippocampal populations examined suggests changes are likely cell type specific within each hippocampal subregion, with each neuronal population having unique drivers of pathology.

Triplicated DEGs in spatially characterized hippocampal neurons

To determine whether genes triplicated in trisomic mice drive dysregulation in hippocampal neuron populations, DEGs from each neuronal population were queried. To fully comprehend the effect of the Ts triplicated chromosome, HSA21 orthologs as well as the non-homologous triplicated region (Mmu17q1a; orthologous to HSA6) were analyzed in the Ts mouse model. A significant subset of triplicated genes was both expressed (63 in CA1 PNs, 66 in CA3 PNs, 65 in DGCs: Supplementary Tables S4–S6) and significantly dysregulated in the three hippocampal neuronal populations. Interestingly, CA1 PNs showed the fewest significant triplicated DEGs (27), while CA3 PNs had the most with 51 triplicated DEGs. DGCs had 35 DEGs from the HSA21 triplicated region (Figure 3F, left panel). Only 1 DEG, Purkinje cell protein 4 (*Pcp4*) was significantly downregulated in CA3 PNs, but upregulated in DGCs, while 18 triplicated DEGs were significantly upregulated by genotype in all three neuronal populations (Figure 3F, left panel). To examine dysregulation of the non-disjunctive region (Mmu17q1a) this chromosomal region was queried for DEGs by genotype in the 3 neuronal populations. Upregulation of 6 DEGs in all three hippocampal neuron populations was observed, along with multiple additional non-disjunctive triplicated DEGs upregulated in one or more of the CA1 PN, CA3 PN, and DGC populations (Figure 3F, right panel). Replicating the orthologs, CA1 PNs had the fewest non-orthologous significant DEGs while CA3 PNs had the largest number of upregulated DEGs from Chr17q1A. This suggests triplication in hippocampal neurons may, in part, drive pathology and behavioral changes seen in DS mice, irrespective of whether it is orthologous or disjunctive.

Mechanistic circuitry dysfunction beyond the DS triplicated region

While many triplicated gene candidates were dysregulated in these three hippocampal neuronal populations, triplicated DEGs represent a small minority (<5%) of total DEGs for any of the excitatory neuronal populations examined. To determine mechanistic pathways driving functional dysregulation in the Ts mouse model, IPA and GO analysis were performed using DEGs from each hippocampal population. Not surprisingly, IPA analysis mimicked the DEGs themselves, exhibiting uniquely dysregulated pathways for the majority of canonical pathways in CA1 PNs, CA3 PNs, and DGCs in trisomic mice (Figure 4A). Where pathways did overlap between CA1 PNs, CA3 PNs and DGCs, the activity was often divergent, indicating differential mechanisms of action (by z-score; Supplementary Tables S7–S9). Select pathways altered in CA1 PNs included downregulation in nonsense-mediated decay and RNA translation, initiation, and termination, concomitantly with upregulation of SNARE signaling, Tricarboxylic acid and respiratory electron transport, and mitochondrial protein import (Figure 4B). These findings suggest at ~6 MO trisomic CA1 PNs have increased neuronal biogenetic activity. In contrast, CA3 DEGs resulted in upregulation of approximately 80% of the canonical pathways (Supplementary Table S8). Unique pathways included upregulation of cholesterol pathways, beta-catenin independent WNT signaling, and myo-inositol biosynthesis pathways, while downregulated pathways included oxidative phosphorylation, insulin processing and DNA methylation (Figure 4C). These findings suggest CA3 PNs are selectively undergoing oxidative stress and degeneration (Kang et al., 2023; Bayona-Bafaluy et al., 2021; Lind et al., 2020). DGCs, like CA3 PNs, displayed approximately 70% of neuronal pathways were upregulated (Supplementary Table S9). Unique to DGCs, these pathways included neuroprotective pathways such as upregulation of NGF signaling, amyloid processing and mitochondrial translation, with downregulation of nNOS signaling and HIF1α signaling (Figure 4D), suggesting DGCs are exhibiting resilience in trisomic mice.

To determine if specific DEGs were driving multiple pathways, the select CA1 unique pathways were analyzed for driver DEGs. CA1 PNs had 12 driver ribosomal DEGs involved in 5 of the select processes. We highlight ribosomal protein L12 (*Rpl12*) as a representative DEG (Figure 4E). There was little overlap in the remaining pathways, with unique DEGs linking two pathways, with limited overlap between genes and pathways (Figure 4E). CA3 PNs showed a similar outcome. We note each representative DEG underlies 2+ DEGs for each subset of interacting processes (Figure 4F). DGCs exhibited a more centralized pattern of driver DEGs and dysregulated processes, with three driver DEGs involved in six or more of the DG unique pathways, with the two other driver DEGs involved in fewer (4) dysregulated pathways (Figure 4G).

A total of 29 pathways were dysregulated in all three cell types (<25%), when canonical neuronal pathways were interrogated (Figure 5A). To determine activation status, pathways were broken down into convergent (all three upregulated or downregulated by z-score), or divergent, (z-score activation indicating upregulation and downregulation dependent on the cell type). The majority of pathways were divergent in CA1 PNs, CA3 PNs, and DGCs. However, neuroinflammation and PPARα/RXRα activation were convergently upregulated in all three (Figure 5B). Dependent on the pairwise comparison, the divergent overlapping pathways could be considered both convergent and divergent, including mitochondrial dysfunction, which was upregulated in CA1 and CA3 PNs and downregulated in DGCs, GABAergic receptor signaling, which was uniquely downregulated in CA3 PNs while upregulated in CA1 PNs and DGCs, and autophagy which was downregulated in CA1 PNs but upregulated in CA3 PNs and DGCs (Figure 5B).

Pathways indicating unique activation status for all three hippocampal neuronal populations included calcium signaling, which had z-scores of zero for both CA1 and CA3 PNs, indicating there was no clear upregulation or downregulation, but z-scores indicated this pathway was downregulated in DGCs. Similarly, $p75^{NTR}$ receptor signaling showed a z-score indicating downregulation of this pathway in CA1 PNs, no clear activity pattern in CA3 PNs (z-score

10.3389/fnmol.2025.1546375

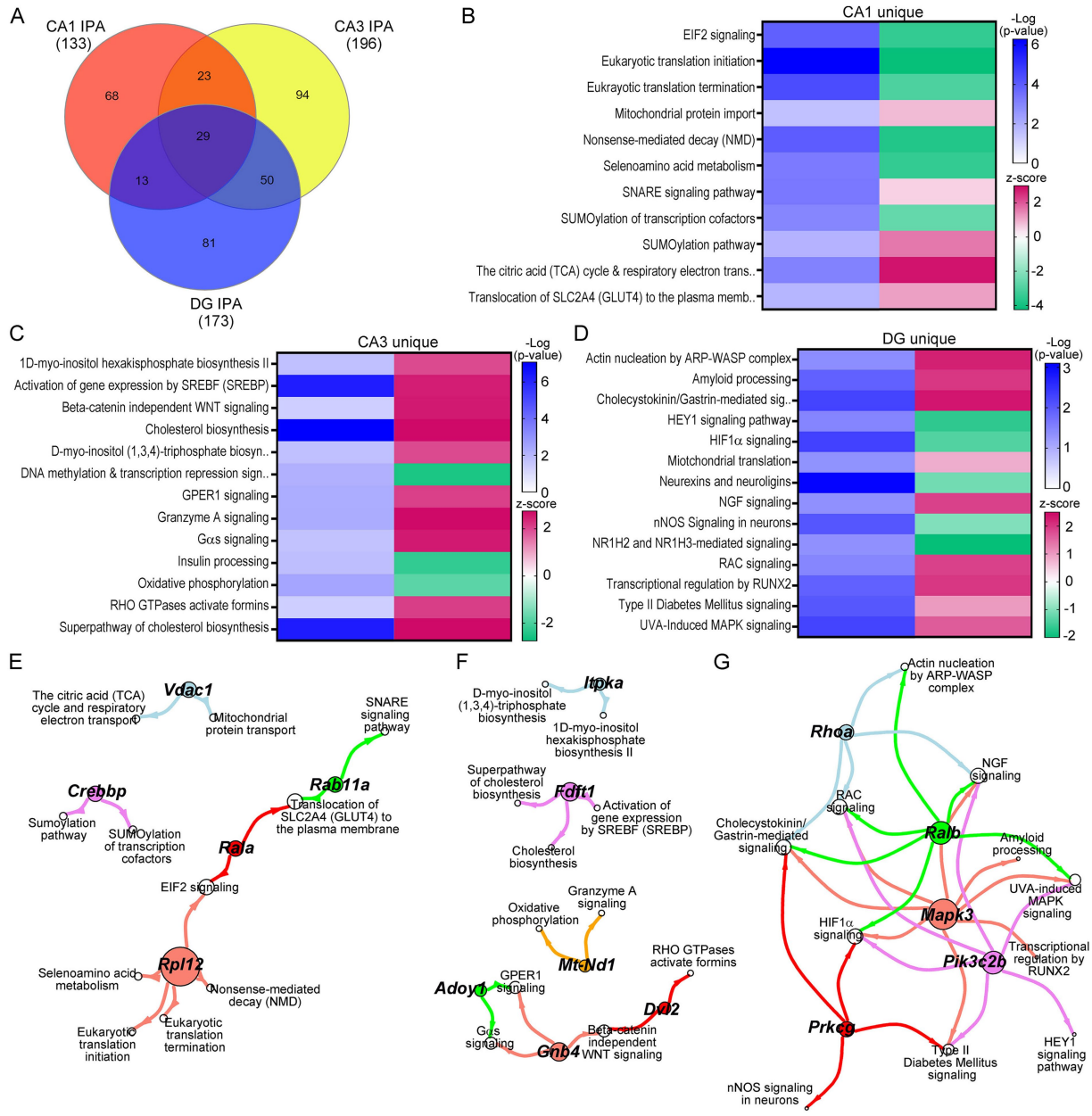

FIGURE 4
IPA was performed on DEGs for each neuron population. **(A)** Venn diagram indicates a subset of the neuronal pathways overlap between CA1 PNs, CA3 PNs, and DGCs. **(B–D)** Heatmaps of select pathways unique to CA1 PN DEGs **(B)**, CA3 PN DEGs **(C)**, and DGC DEGs **(D)** depict regulation by z-score (upregulated pink, downregulated green), with significance judged using –Log(*p*-value) in shades of blue. **(E–G)** Spiral graphs display top DEGs involved in selected CA1 **(E)**, CA3 **(F)**, and DG **(G)** unique pathways showing little overlap of driver DEGs and select pathways.

of 0), and upregulation in DGCs (Figure 5B). To determine whether DEGs themselves reflect why these activation scores are so diverse, driver DEGs were examined. Each neuronal population was examined for drivers of these overlapping pathways (Figure 5B), in many cases this was caused by a unique subunit or isoform dysregulation in trisomic mice. CA1 PNs (Figure 5C), CA3 PNs (Figure 5D), and DGCs (Figure 5E) each display unique genes driving the same dysregulated pathways selected from 29 overlapping pathways. A few DEGs overlapped, including guanine nucleotide binding protein, alpha stimulating (*Gnas*), which was upregulated in CA1 and CA3 PNs, but not significantly in DGCs. *Gria2* is downregulated in CA3 PNs and DGCs but is not significantly in CA1 PNs.

Neurological Disesae and Functional analysis via IPA reveals molecular phenotypes of unique hippocampal neuron populations

Analysis of D/Fs in IPA was restricted to neurological and cellular D/Fs, which revealed behavioral processes and underlying

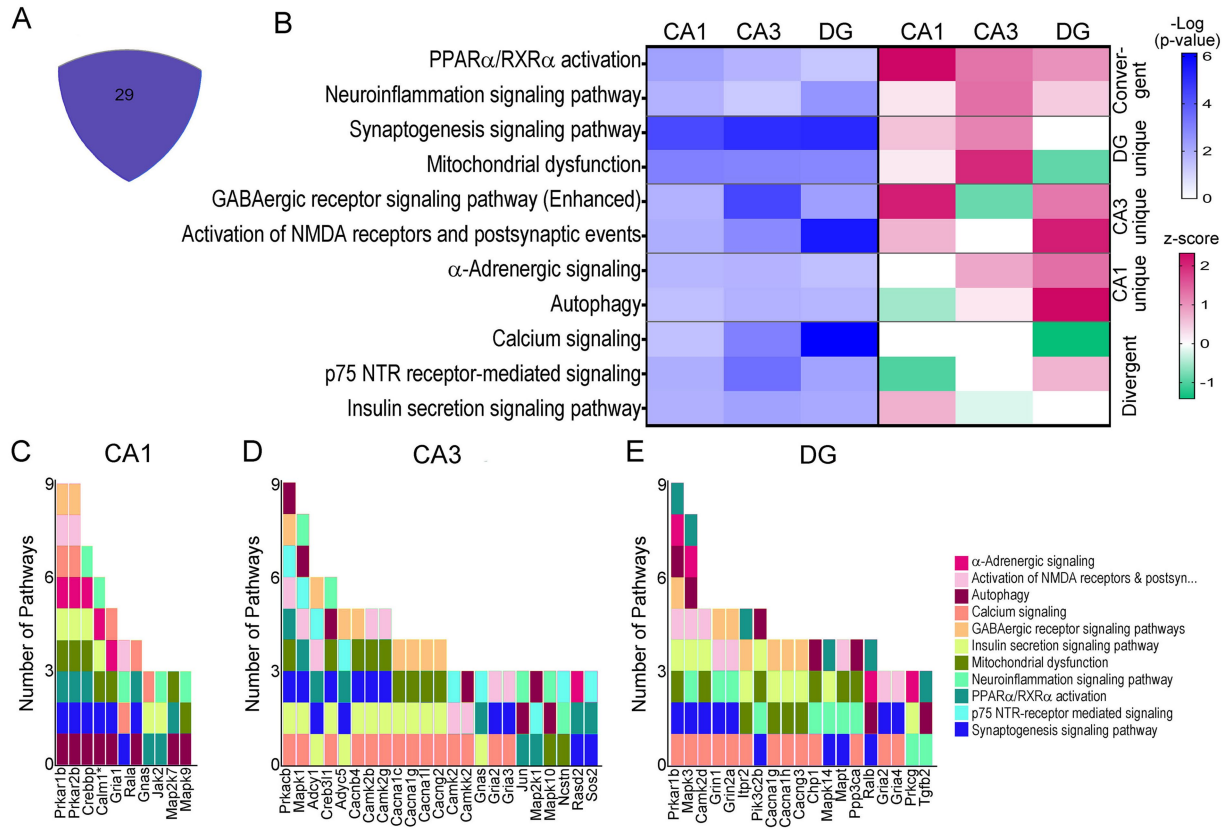

FIGURE 5
IPA pathways dysregulated in all three neuronal populations. **(A)** Central area of Venn diagram (Figure 4A) highlights the 29 convergently dysregulated pathways. **(B)** In selected overlapping pathways, −Log *p*-value shows significant dysregulation of the convergent pathways by activation score (z-score, pink = upregulation; green = downregulation) **(C–E)** Stacked bar charts show CA1 PN DEGs **(C)**, CA3 PN DEGs **(D)**, and DGC DEGs **(E)** involved in overlapping pathways on the *x*-axis of a bar chart with the *y*-axis linking pathways involved to each DEG. * includes others in CA1 PNs (per the IPA program).

cellular mechanisms both unique and convergently dysregulated in trisomic hippocampal neuronal populations. Activation z-scores are based on DEGs in the pathway and the reported effect this dysregulation has on the activity of the specific D/F, as determined by the IPA program. Similar to the canonical pathways, many D/Fs were uniquely dysregulated based on the DEG expression, as determined by IPA analysis. Several key behavioral and cellular functions were also dysregulated in all three hippocampal neuron subtypes, including downregulation of learning and LTP and upregulation of progressive neurological disorder (Figure 6A; Supplementary Tables S10–S12). Interestingly, spatial memory was uniquely upregulated in 6 MO trisomic CA1 PNs and downregulated in CA3 PNs and DGCs. Conversely, the D/F termed "memory" was downregulated in CA1 PNs and CA3 PNs and moderately upregulated in DGCs (Figure 6A). Several other D/Fs were only significantly dysregulated in one cell type, including downregulation of autophagy and upregulation of fission of mitochondria in CA1 PNs (Figure 6B; Supplementary Table S10). Trisomic CA3 PNs displayed unique upregulation of amyloidosis and synthesis of cholesterol and downregulation of cued conditioning and repression of RNA (Figure 6C; Supplementary Table S11). DGCs uniquely displayed downregulation of nociception and upregulation of startle response and aggregation of mitochondria (Figure 6D; Supplementary Table S12).

GO analysis confirms dysregulation is hippocampal cell-type specific

GO processes, including biological processes, cellular components and molecular functions were analyzed in CA1 PNs, CA3 PNs and DGCs by genotype. Dysfunctional processes were binned into 14 categories (Supplementary Figure S4; Supplementary Tables S13–S15) and analyzed for overlapping or unique processes (Figure 7). CA1 PNs exhibited limited overlap of dysregulated processes with DGCs (7% of total CA1, 8% of total DGCs). In contrast, CA3 PNs showed a higher percentage of overlapping dysregulated processes with DGCs (17% of total CA3 and 25% of total DGCs). DGCs had the most overlapping dysregulated processes (36% of total DGCs), coinciding with the fewest unique dysregulated processes by genotype (31% of total DGCs). Dysregulated trisomic CA1 PNs processes overlapped ~3.5 times more with CA3 PNs than with DGCs. CA3 PNs showed similar percentages of overlap with DGCs or CA1 PNs, although trisomic CA3 PNs had the

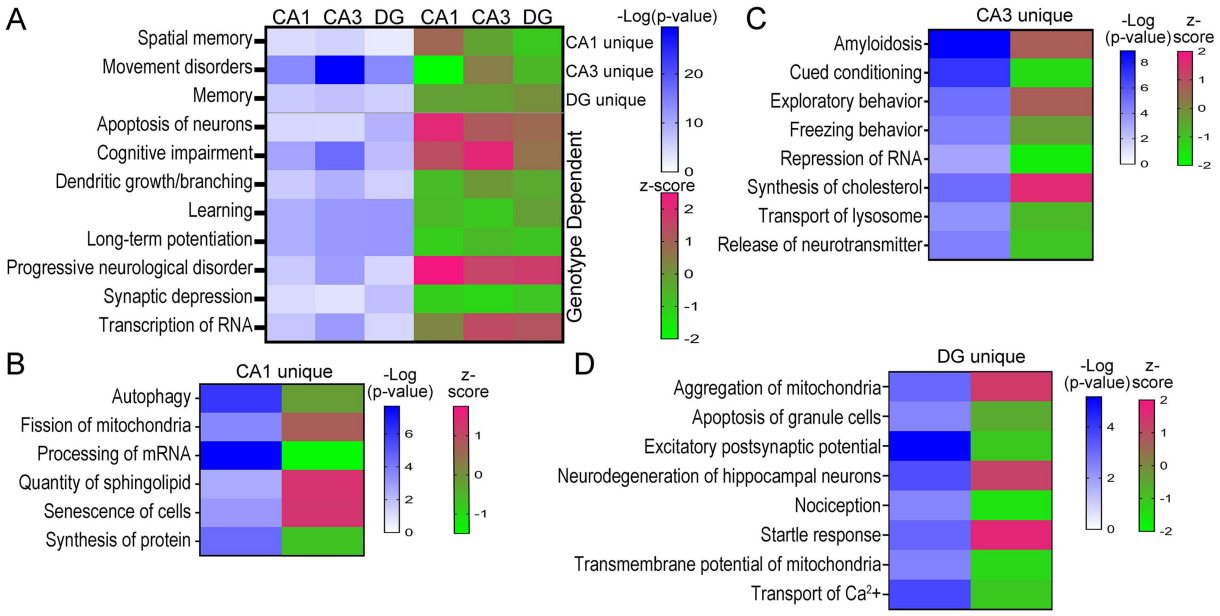

FIGURE 6
D/Fs in the three hippocampal populations showed neurological deficits in trisomic mice. **(A)** Heatmaps illustrate D/Fs dysregulated in all three neuron populations with significance in shades of blue and activation in shades of pink (upregulated) and green (downregulated). **(B–D)** Select CA1 **(B)**, CA3 **(C)**, and DG **(D)** unique D/Fs are shown by a heatmap indicating significance and activation.

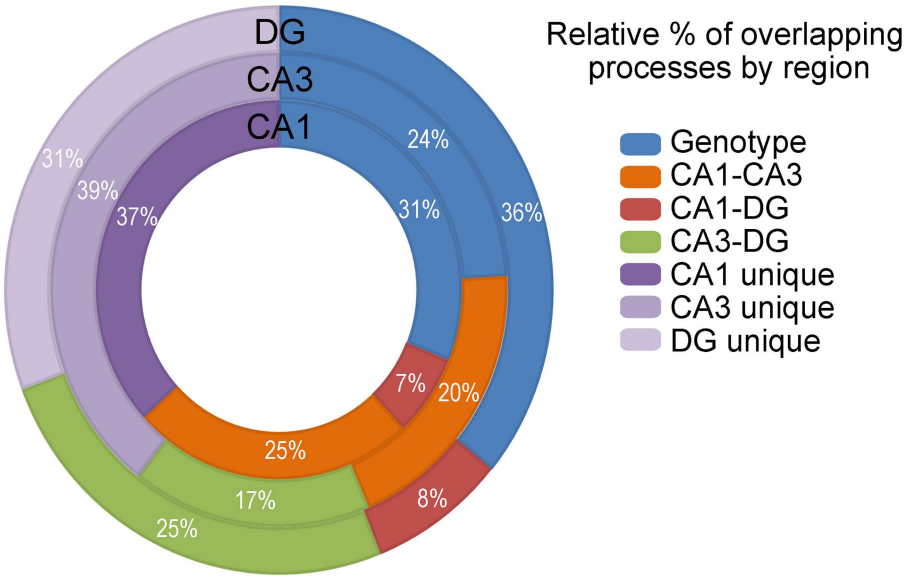

FIGURE 7
GO analysis was performed and analyzed in the DGCs (outer circle), CA3 PNs (middle circle) and CA1 PNs (inner circle) by genotype (blue), CA1-CA3 overlapping processes (orange), CA1-DG overlapping processes (red), CA3-DG overlapping processes (green), and cell type unique processes (shades of purple). Activation is not accessible in GO analysis. Overlapping processes are assessed and presented.

most unique dysregulated processes. Like IPA, GO analysis indicated a significant minority (31–39%) of dysregulated processes were completely excitatory cell type specific. IPA and GO analysis results in many more pathways and processes driving pathological changes by genotype, while DGC mechanisms appear to be more disparate, suggesting trisomic CA1 and CA3 PNs may drive hippocampal dysregulation concomitantly.

Protein validation of APP and DYRK1A dysregulation

Two triplicated DEGs were interrogated for protein expression, namely APP and DYRK1A. Both were upregulated in all three hippocampal cell types. *App* displayed varied LFCs with CA1 PNs

showing the smallest LFC (Supplementary Table S1, LFC = 0.271), while CA3 PNs and DGCs exhibited larger LFCs (Supplementary Tables S2, S3; LFC of 0.621 and 0.736 respectively). *Dyrk1a*, however, had similar LFCs across all three cell types (LFC range 0.392–0.541; Supplementary Tables S1–S3). At the protein level, APP replicated this pattern with a smaller, but significant, increase in protein expression (~1.59 fold) in CA1 sector enriched tissue (Figure 8A). The CA3 sector + DG enriched dissection also showed significantly increased APP expression by genotype (~1.8-fold, Figure 8A). Regional differences were not seen in APP expression for 2N mice. However, trisomic mice showed significant regional upregulation in the CA3 sector + DG dissection versus the CA1 sector (Figure 8A). β-CTF fragments did not reach statistical significance in either the CA1 sector or CA3 sector + DG dissection (Figure 8B). Similar to APP, the CA3 sector + DG dissection displayed a trend for higher expression of β-CTF compared to the CA1 sector in both 2N ($p = 0.072$) and Ts ($p = 0.066$; Figure 8). DYRK1A showed high variability in the CA1 sector, resulting in no significant difference in protein expression by genotype. Significant upregulation of DYRK1A was observed in the CA3 sector + DG dissection in trisomic mice (Figure 8). No significant differences were seen between the CA1 sector and the CA3 sector + DG dissection in 2N mice. Similar to APP protein expression, DYRK1A exhibited lower expression in the CA1 sector compared to the CA3 sector + DG dissection in trisomic mice (Figure 8, $p < 0.0031$). The protein assays were conducted in subregional dissections containing admixed cell types. Results show elevated APP expression suggesting expression increases in both neuronal and non-neuronal (e.g., astrocyte and/or microglia) populations which has been previously seen after neuronal damage (Zhao et al., 2011). However, DYRK1A protein expression increases are partially masked, which may suggest DYRK1A expression is neuron specific, as previously described in postmortem human tissue (Wegiel et al., 2004). Overall, triplicated protein expression appears to mimic alterations in RNA expression in the trisomic model.

Discussion

RNA-seq analysis of Ts65Dn mice in three hippocampal excitatory neuronal populations resulted in unique differences in gene expression in CA1 PNs, CA3 PNs, and DGCs. CA3 PNs showed the most profound dysregulation, with more DEGs (Figure 2; Supplementary Table S2), resulting in higher numbers of dysregulated canonical pathways and processes by genotype (Supplementary Tables S8, S11, S14). Transcriptomic data corroborates previous studies showing dysregulation of CA3 mEPSCs in the Ts65Dn mouse model (Hanson et al., 2007;

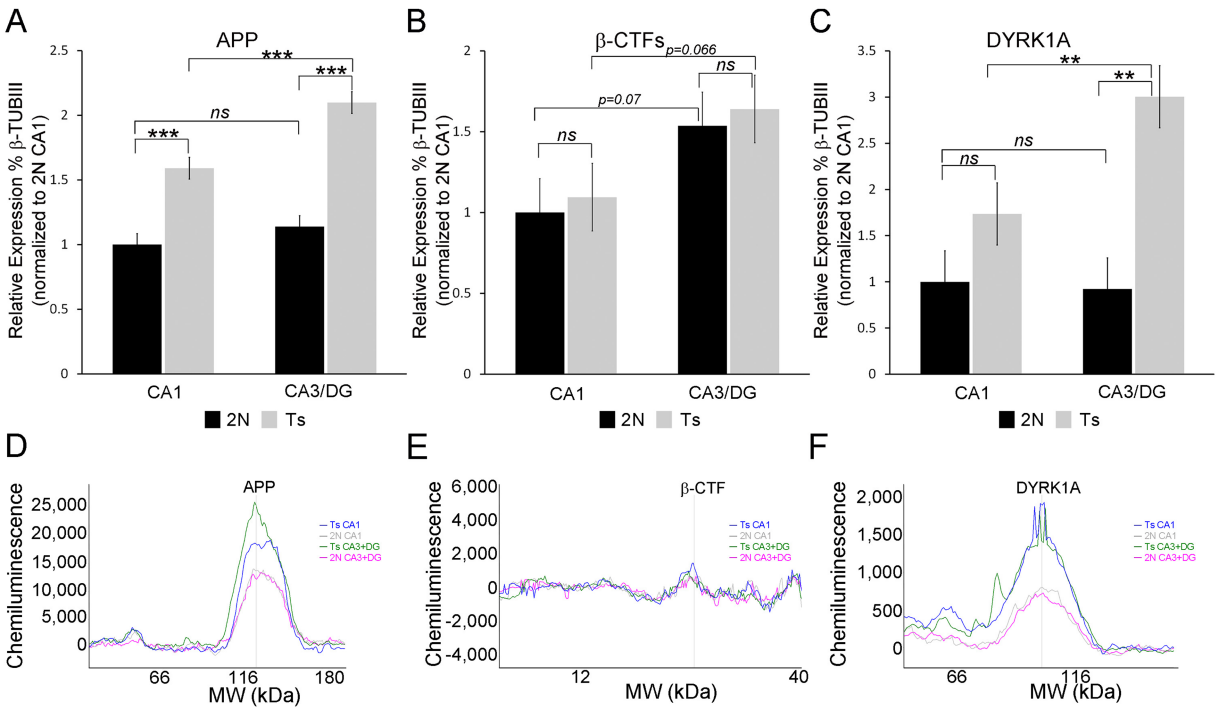

FIGURE 8
Protein validation was performed on CA1 sector and CA3 sector + DG enriched tissue from the same mice utilized for single population RNA-seq, with the exception of one novel age matched 2N brain as described in the methods **(A)**. APP is upregulated in Ts compared to 2N in both the CA1 sector and CA3 sector + DG enriched dissection. 2N mice showed no difference in expression between regions, while Ts mice showed significant upregulation in CA3 sector + DG compared to CA1. **(B)** β-CTF levels were not significantly different by genotype. A trend level upregulation was found comparing the CA1 sector to CA3 sector + DG enriched dissection. **(C)** DYRK1A expression was not significantly different in the CA1 sector. Significant upregulation was found by genotype in the CA3 sector + DG enriched dissection. Upregulation of DYRK1A expression was also observed in the CA3 sector + DG enriched dissection compared to the CA1 sector in trisomic mice. Proteins were assessed relative to 2N β-TubIII levels and normalized to mean 2N CA1 sector expression. **(D–F)** Representative traces of WES analysis for Ts CA1 (blue), 2N CA1 (grey), Ts CA3 + DG (green), and 2N CA3 + DG (pink) are shown for APP **(D)**, β-CTFs **(E)**, and DYRK1A **(F)**. Key: ***$p < 0.001$, **$p < 0.01$, trend levels were presented as p-values; ns, not significant.

Stagni et al., 2013), with transcriptomic analysis indicating specific upregulation of NMDA receptors and downregulation of GABAergic signaling (Figure 5B). However, to date no studies replicated this excitatory effect in CA1 PNs or DGCs. Upregulation of HSA21 orthologs as well as non-homologous triplication of Mmu17 genes were seen in all three neuronal populations, with unique as well as convergent dysregulation of a subset of the triplicated region (Figure 3F). Thus, our in-depth analysis of CA1 PNs, CA3 PNs, and DGCs by genotype resulted in key transcriptomic differences associated with signaling and circuitry alterations in this DS/AD model.

To determine the effect of triplication on gene expression throughout the hippocampal excitatory neuron network, DEGs for each neuronal type were examined for HSA21 orthologs. Increased expression in one or more neuronal populations was seen for a significant subset of the triplicated orthologs, as seen previously (Sierra et al., 2024). Interestingly, half of the 31 convergent DEGs in the three hippocampal cell types (Figure 3B) were HSA21 orthologs (Figure 3F). This included *App* and *Dyrk1a,* which were further examined for protein expression. Previous studies using trisomic mouse hemibrains found disomic APP levels were maintained until ~8 MO (Choi et al., 2009), while microarray analysis revealed upregulation of *App* CA1 PNs in older (10+ MO) but not 6 MO Ts65Dn mice (Alldred et al., 2015b; Alldred et al., 2015a). These prior studies suggest hippocampal APP protein levels are increased at an earlier timepoint than the rest of the brain. Although these findings were not observed by microarray analysis (Alldred et al., 2015a), the higher sensitivity of RNA-seq based assays allows for the statistically significant identification of small increases, as seen in a recent single nucleus RNA-seq analysis (Sierra et al., 2024). However, clinical trials with treatments (e.g., immunotherapies) targeting Aβ have equivocal results in regard to cognitive benefits in AD dementia (Solopova et al., 2023; Ebell et al., 2024; Digma et al., 2024). We postulate the mechanisms driving DS/AD pathology result from additional factors beyond APP triplication (Mufson et al., 2021; Alldred et al., 2024b; Alldred et al., 2024a). In this regard, intellectual disabilities, linked to hippocampal *Dyrk1a* overexpression, are ameliorated when *Dyrk1a* expression is reduced in DS mouse models (Altafaj et al., 2013; Dowjat et al., 2007; Feki and Hibaoui, 2018). Significant DYRK1A encoded protein upregulation was seen in the CA3 sector + DG tissue, along with increased RNA expression seen in all three hippocampal neuronal populations. We postulate the DYRK1A protein is upregulated in neurons throughout the hippocampus and is causal to memory impairments. Support comes from studies that show adult human neurons exhibit higher expression levels of DYRK1A compared to relatively low expression levels in glial populations in normal postmortem brain tissue (Wegiel et al., 2004). Moreover, DYRK1A expression is upregulated within excitatory cortical PNs of individuals with DS (Alldred et al., 2024b).

We noted 5 of the 31 convergent DEGs were HSA6 orthologs, homologous to the non-disjunctive triplicated region of Mmu17, fragment 1A (Chr17q1A; Figure 3F; Duchon et al., 2011), indicating off target upregulation is also seen in these hippocampal neurons. However, while a large subset of triplicated DEGs were identified from each neuronal subtype, accounting for the majority of convergent DEGs overall, these DEGs represent a minor fraction of the total dysregulation observed in trisomic neurons, thus we concentrated on studying gene expression beyond triplicated HSA21 orthologs.

To examine genotype and circuitry effects on cellular mechanisms, DEGs were examined using IPA and GO analysis. Many pathways and processes overlapped between neuronal populations. However, unique gene expression changes often underlie these dysregulated pathways in trisomic mice, with alternative subunits or isoforms dysregulated in each neuronal population. For example, the top genes dysregulated in 9 convergent IPA pathways in trisomic CA1 PNs were protein kinase cAMP-dependent type I regulatory subunit beta (*Prkar1b*; Figure 5C) and protein kinase cAMP-dependent type II regulatory subunit beta (*Prkar2b*; Figure 5C), while in the CA3 PNs, the top gene dysregulated in those same 9 pathways was protein kinase cAMP-activated catalytic subunit beta (*Prkacb*; Figure 5D). Subunit specificity of the protein kinase A (PKA) holoenzyme modulates subcellular targeting and PKA functional specificity (Omar and Scott, 2020). This suggests secondary regulation is highly specialized in each trisomic hippocampal neuron population, each with their own intrinsic vulnerabilities. This example is one of many DEGs displaying subunit specificity for common pathways dysregulated based on the spatial localization and circuitry differences from excitatory hippocampal neurons. We postulate dysregulation of cellular mechanisms is dependent on innervation and circuitry activation in the hippocampus, especially from the perforant path and BFCNs, driving unique behavioral alterations and neurological functions (Mufson et al., 2016; Ginsberg, 2010; Ginsberg et al., 2006; Alldred et al., 2024a; Alldred et al., 2023; Alldred et al., 2021c).

IPA analysis revealed many D/Fs were population specific. CA1 PNs showed upregulation of spatial memory, while CA3 PNs and DGCs DEGs resulted in downregulation of this pathway by genotype (Figure 6A), indicating gene expression alterations are compensatory for spatial memory functions within CA1 PNs. Although CA1 PNs are thought to drive spatial memory and consolidation of spatial memory as part of the septohippocampal circuit (Ash et al., 2014; Velazquez et al., 2013; Al-Onaizi et al., 2017; Perez-Cruz et al., 2011), increased cholinergic tone in Ts65Dn mice by ~7–8 MO has also been suggested to be a compensatory mechanism for the progressive increase in dysfunction similar to prodromal AD (Kelley et al., 2016). BFCN innervation to the CA1 sector may preserve or compensate for degeneration at this younger age. Together, we postulate connectivity-based alterations in the septohippocampal circuit drive memory, specifically spatial memory alterations, associated with CA1 neurons, which is preserved early, but ultimately is lost during the progression of BFCN degeneration in trisomic mice (Alldred et al., 2021c).

We link unique pathways and processes significantly dysregulated in CA1 PNs, CA3 PNs, and DGCs to previous behavioral assessments. IPA predicts DEGs in CA3 PNs will drive increased exploratory behavior, which coincides with increased amyloidosis (Figure 6), suggesting CA3 PNs are degenerating, as trisomic mice have previously been shown to have impaired fear conditioning by 4–6 MO (Costa et al., 2008). Fear conditioning is partially rescued by the NMDA receptor antagonist, memantine, by increasing activity of excitatory neurons (Costa et al., 2008). This corroborates the link between impaired excitatory CA3 PNs and behavioral deficits previously seen in trisomic mice. IPA and GO analyses reveal CA3 PNs have a robust degenerative phenotype, with DEGs and memory-related processes downregulated, suggesting CA3 PNs are significantly impaired at this early timepoint. DGCs display decreases in excitatory postsynaptic potential (Figure 7D). Previous studies suggest this decrease is due to overinhibition driven by inhibitory neuron signaling within the DG (Kleschevnikov et al., 2004; Kleschevnikov et al., 2012b). However, DEGs identified in the D/F "Excitatory postsynaptic potential" were heavily linked to dsyregulation of AMPA/NMDA receptor subunits (Supplementary Table S12), as

expected when exclusively profiling excitatory neuron populations. Further, trisomic mice exhibited genotype dependent decreased LTP (Figure 6A) in all three excitatory neuron populations. Decreased LTP has been associated with an excitatory/inhibitory imbalance (Kleschevnikov et al., 2012b; Kleschevnikov et al., 2004; Costa and Grybko, 2005; Chakrabarti et al., 2010). We posit that both excitatory and inhibitory neurons have dysfunctional gene expression changes that cumulate in mechanistic alterations of cellular functions, which underlie degeneration in this well-established DS/AD model. Further study of trisomic inhibitory neurons is required to corroborate these findings.

Molecular hallmarks of the DS degenerative phenotype are seen in Ts65Dn mice, with profound deficits within MSN BFCNs (Alldred et al., 2023) as well as a mosaic of deficits in the three populations of hippocampal excitatory neurons. When examining septohippocampal circuit neurons, hippocampal excitatory neurons show many more triplicated DEGs compared to MSN BFCNs (Alldred et al., 2023), suggesting genotype effects from triplication are more profound within hippocampal excitatory neurons compared to BFCNs. In contrast, total DEGs and the underlying mechanistic pathways dysregulated in Ts65Dn mice are more profound in MSN BFCNs (Alldred et al., 2023), compared to the hippocampal neuron populations. Early deficits, including increased neuroinflammation and reactive oxygen species generation, are seen in both MSN BFCNs and hippocampal neurons by 6 MO, along with synaptic and metabolic deficits, which are much more profound in BFCNs (Alldred et al., 2023), suggesting BFCN dysregulation precedes or paces hippocampal neurons deficits via connectivity-based neurodegeneration. This is corroborated by previous studies in human AD and DS (Yates et al., 1980; Whitehouse et al., 1982) and DS mice (Granholm et al., 2000; Kelley et al., 2014a; Lockrow et al., 2009), which display profuse age-dependent BFCN degeneration. Further, degeneration of the basal forebrain occurs prior to the entorhinal cortex in AD (Fernández-Cabello et al., 2020). We postulate that early targeting of BFCNs likely would slow or stop the onset of hippocampal degeneration.

Caveats and future directions

We strive to limit LCM and RNA variability by normalizing quality and quantity during bioinformatic analysis. Sex differences exist in AD pathology and this study lacks female animals, which results in the inability to determine sex effects. We plan to ameliorate this deficit utilizing a female cohort, age-and sex matched to the males performed herein, although sex effects have not been noted in human DS RNA-seq in cortical excitatory neurons (Alldred et al., 2024b). To isolate genotype specific differences driven solely by BFCN degeneration, it would be advisable to utilize a younger cohort prior to frank neurodegeneration. Further, new models of DS (e.g., TcMAC21 mouse) (Kazuki et al., 2020; Shao et al., 2023) have been developed that reproduce triplication of virtually all HSA21 orthologs, which may result in unique DEGs not seen herein. Additional planned assessments include examining the therapeutic modality of maternal choline supplementation in hippocampal cell types, as trisomic BFCNs display notable benefits and reduction of dysregulated DEGs and pathways in the Ts65Dn model (Alldred et al., 2023). We also propose examining GABAergic interneurons in the septohippocampal circuit for deficits in the context of DS/AD.

Conclusion

Using single population profiling, we analyzed alterations in an established DS/AD model at the onset of septohippocampal degeneration and identified genotype and circuitry specific alterations. As expected, each excitatory population had a unique expression profile, but unexpectedly, few genes exhibited convergent dysregulation in excitatory neurons throughout the hippocampus in trisomic mice. We postulate unique gene expression within each circuit drives pathology in the DS brain. Interestingly, CA3 PNs exhibited the most robust dysregulated gene expression profile, while CA1 PNs and DGCs exhibited fewer dysregulated DEGs. Overall, bioinformatic analysis indicated significant overlap in pathway dysregulation were associated with unique DEGs, suggesting isoform and/or subunit specificity is linked to circuitry and/or expression to individual hippocampal neuronal populations, which has translational implications for human DS and informs on AD dementia. Bioinformatic inquiry of CA1 PN, CA3 PN, and DGC DEGs delineated unique drivers of disease pathology and linked select behavioral deficits to individual excitatory neuronal populations dysregulated in trisomic mice. We propose unique gene expression changes may drive similar outcomes in different neuronal populations through distinct regulation of signaling cascades, which in turn suggests precision targeting for therapeutic modulation of degeneration may be necessary for DS/AD degeneration.

Data availability statement

The datasets presented in this study can be found in online repositories. The names of the repository/repositories and accession number(s) can be found in the article/Supplementary material. RNA-seq data analyzed within this study are available from GEO (http://www.ncbi.nlm.nih.gov/geo; GSE283699).

Ethics statement

The animal study was approved by Nathan Kline Institute/New York University Grossman School of Medicine. The study was conducted in accordance with the local legislation and institutional requirements.

Author contributions

MJA: Conceptualization, Data curation, Formal analysis, Investigation, Methodology, Project administration, Supervision, Validation, Visualization, Writing – original draft, Writing – review & editing. KWI: Data curation, Formal analysis, Methodology, Software, Visualization, Writing – original draft, Writing – review & editing. HP: Formal analysis, Software, Visualization, Writing – original draft, Writing – review & editing. SHL: Writing – original draft, Writing – review & editing, Data curation, Formal analysis. AH: Methodology, Writing – original draft, Writing – review & editing, Resources. GC: Conceptualization, Writing – original draft, Writing – review & editing. EJM: Conceptualization, Investigation, Supervision, Writing – original draft, Writing – review & editing. GES: Conceptualization, Funding acquisition, Resources, Writing – original draft, Writing – review & editing. SDG: Conceptualization, Funding acquisition, Investigation,

Methodology, Project administration, Resources, Supervision, Validation, Writing – original draft, Writing – review & editing.

Funding

The author(s) declare that financial support was received for the research, authorship, and/or publication of this article. Funding was provided by support from grants AG014449, AG072599, AG081286, AG074004, AG077103, and AG085572 from the National Institutes of Health.

Acknowledgments

We thank Arthur Saltzman for technical support and Elise Webber for assistance with manuscript editing.

Conflict of interest

The authors declare that the research was conducted in the absence of any commercial or financial relationships that could be construed as a potential conflict of interest.

The author(s) declared that they were an editorial board member of Frontiers, at the time of submission. This had no impact on the peer review process and the final decision.

Generative AI statement

The authors declare that no Gen AI was used in the creation of this manuscript.

Publisher's note

Supplementary material

The Supplementary material for this article can be found online at: https://www.frontiersin.org/articles/10.3389/fnmol.2025.1546375/full#supplementary-material

SUPPLEMENTARY FIGURE S1
(A–C) Gene expression analysis using voom showed mean-variance trends at a stringency of 10 for isolation of DEGs by genotype in CA1 PNs **(A)**, CA3 PNs **(B)**, and DGCs **(C)**. **(D)** MDS plots for CA1 PNs show inter-and intra-group variability for 2N (light red) and Ts (dark red) per subject. **(E)** CA3 PNs MDS with 2N (light blue) and Ts (dark blue) dots per subject. **(F)** DGCs MDS plot shows 2N (light green) and Ts (dark green) variability per subject.

SUPPLEMENTARY FIGURE S2
Normalized cell counts were assayed to determine gene expression for markers of eight different cell types (Mathys et al., 2023). **(A–C)** LCM microisolated hippocampal neurons showed significantly higher expression for excitatory neuron (ExcN) expressing genes compared to genes identified as expressing specifically in inhibitory neurons (InhN), astrocytes (Astro), oligodendrocytes (oligo), oligodendrocyte progenitor cells (OPC), microglia (MG), endothelial cells (Endo), and T-cells (T). CA1 **(A)** $p < 0.0001$ for all comparisons. No significant difference was seen between ExcN expression by genotype ($p = 0.4382$). CA3 PNs **(B)** 2N $p < 0.0001$ for all comparisons; Ts $p < 0.0011$ or lower for all comparisons. No significant difference was seen between ExcN expression by genotype ($p = 0.2594$). **(C)** DGCs $p < 0.0001$ for all comparisons. No significant difference was seen between ExcN expression by genotype ($p = 0.7071$).

SUPPLEMENTARY FIGURE S3
STRING in Cytoscape analysis was performed on all DEGs by cell type and genotype. **(A)** Of the 948 DEGs, STRING identified 890 proteins to examine for PPI analysis. Clusters show significant overlap of PPI s of CA1 PNs DEGs, with few DEGs showing none or only 1 interacting partner. **(B)** Of the 1,566 DEGs in CA3 PNs, STRING found 1,482 proteins for PPI analysis. Clusters show significant overlap of PPI interactions of CA1 DEGs, with CA3 DEGs showing the lowest number of proteins with 1 or no interacting partners. **(C)** Of the 692 DGCs DEGs, 658 proteins were queried for PPI analysis. DGCs had the highest total number of proteins showing no or one interaction with the other proteins queried from the DEGs.

SUPPLEMENTARY FIGURE S4
GO analysis was employed to interrogate DEGs from the three hippocampal neuron populations. **(A)** Processes dysregulated in GO analysis in CA1 PNs were binned by category, with "protein" having relatively more dysregulation (percentage of total dysregulated pathways) compared to CA3 PNs or DGCs. **(B)** CA3 PNs showed similar dysregulation in terms of percentages of processes compared to CA1 PNs, with only slightly higher rates of metabolism and neurotransmitter, ions and receptor (NIR) processes dysregulated, although NIR had a higher percentage in DGCs compared to CA3 PNs. **(C)** DGCs showed relatively more dysregulated developmental processes, more than CA1 or CA3 and a moderately higher relative percentage of signaling processes were dysregulated. Signaling percentage was lowest in CA1 PNs, moderate in CA3 PNs, and highest in DGCs.

SUPPLEMENTARY TABLE S1
List of DEGs for CA1 PNs in Ts compared to 2N at $p < 0.05$.

SUPPLEMENTARY TABLE S2
List of DEGs for CA3 PNs in Ts compared to 2N at $p < 0.05$.

SUPPLEMENTARY TABLE S3
List of DEGs for DGCs in Ts compared to 2N at $p < 0.05$.

SUPPLEMENTARY TABLE S4
List of all triplicated genes expressed in CA1 PNs including orthologs and non-orthologs.

SUPPLEMENTARY TABLE S5
List of all triplicated genes expressed in CA3 PNs including orthologs and non-orthologs.

SUPPLEMENTARY TABLE S6
List of all triplicated genes expressed in DGCs including orthologs and non-orthologs.

SUPPLEMENTARY TABLE S7
List of IPA canonical pathways significantly dysregulated in CA1 PNs in Ts compared to 2N.

SUPPLEMENTARY TABLE S8
List of IPA canonical pathways significantly dysregulated in CA3 PNs in Ts compared to 2N.

SUPPLEMENTARY TABLE S9
List of IPA canonical pathways significantly dysregulated in DGCs in Ts compared to 2N.

SUPPLEMENTARY TABLE S10
List of IPA D/Fs significantly dysregulated in CA1 PNs in Ts compared to 2N.

SUPPLEMENTARY TABLE S11
List of IPA D/Fs significantly dysregulated in CA3 PNs in Ts compared to 2N.

SUPPLEMENTARY TABLE S12
List of IPA D/Fs significantly dysregulated in DGCs in Ts compared to 2N.

SUPPLEMENTARY TABLE S13
Total GO processes sorted by bin of significantly dysregulated in CA1 PNs in Ts compared to 2N.

SUPPLEMENTARY TABLE S14
Total GO processes sorted by bin of significantly dysregulated in CA3 PNs in Ts compared to 2N.

SUPPLEMENTARY TABLE S15
Total GO processes sorted by bin of significantly dysregulated in DGCs in Ts compared to 2N.

References

Ahmed, M. M., Sturgeon, X., Ellison, M., Davisson, M. T., and Gardiner, K. J. (2012). Loss of correlations among proteins in brains of the Ts65Dn mouse model of Down syndrome. *J. Proteome Res.* 11, 1251–1263. doi: 10.1021/pr2011582

Akeson, E. C., Lambert, J. P., Narayanswami, S., Gardiner, K., Bechtel, L. J., and Davisson, M. T. (2001). Ts65Dn – localization of the translocation breakpoint and trisomic gene content in a mouse model for Down syndrome. *Cytogenet. Cell Genet.* 93, 270–276. doi: 10.1159/000056997

Alldred, M. J., Chao, H. M., Lee, S. H., Beilin, J., Powers, B. E., Petkova, E., et al. (2018). CA1 pyramidal neuron gene expression mosaics in the Ts65Dn murine model of Down syndrome and Alzheimer's disease following maternal choline supplementation. *Hippocampus* 28, 251–268. doi: 10.1002/hipo.22832

Alldred, M. J., and Ginsberg, S. D. (2023). Microisolation of spatially characterized single populations of neurons for RNA sequencing from mouse and postmortem human brain tissues. *J. Clin. Med.* 12:3304. doi: 10.3390/jcm12093304

Alldred, M. J., Lee, S. H., and Ginsberg, S. D. (2021a). Adiponectin modulation by genotype and maternal choline supplementation in a mouse model of Down syndrome and Alzheimer's disease. *J. Clin. Med.* 10:2994. doi: 10.3390/jcm10132994

Alldred, M. J., Lee, S. H., Petkova, E., and Ginsberg, S. D. (2015a). Expression profile analysis of vulnerable CA1 pyramidal neurons in young-middle-aged Ts65Dn mice. *J. Comp. Neurol.* 523, 61–74. doi: 10.1002/cne.23663

Alldred, M. J., Lee, S. H., Petkova, E., and Ginsberg, S. D. (2015b). Expression profile analysis of hippocampal CA1 pyramidal neurons in aged Ts65Dn mice, a model of Down syndrome (DS) and Alzheimer's disease (AD). *Brain Struct. Funct.* 220, 2983–2996. doi: 10.1007/s00429-014-0839-0

Alldred, M. J., Lee, S. H., Stutzmann, G. E., and Ginsberg, S. D. (2021b). Oxidative phosphorylation is dysregulated within the basocortical circuit in a 6-month old mouse model of Down syndrome and Alzheimer's disease. *Front. Aging Neurosci.* 13:707950. doi: 10.3389/fnagi.2021.707950

Alldred, M. J., Penikalapati, S. C., Lee, S. H., Heguy, A., Roussos, P., and Ginsberg, S. D. (2021c). Profiling basal forebrain cholinergic neurons reveals a molecular basis for vulnerability within the Ts65Dn model of Down syndrome and Alzheimer's disease. *Mol. Neurobiol.* 58, 5141–5162. doi: 10.1007/s12035-021-02453-3

Alldred, M. J., Pidikiti, H., Heguy, A., Roussos, P., and Ginsberg, S. D. (2023). Basal forebrain cholinergic neurons are vulnerable in a mouse model of Down syndrome and their molecular fingerprint is rescued by maternal choline supplementation. *FASEB J.* 37:e22944. doi: 10.1096/fj.202202111RR

Alldred, M. J., Pidikiti, H., Ibrahim, K. W., Lee, S. H., Heguy, A., Hoffman, G. E., et al. (2024a). Hippocampal CA1 pyramidal neurons display sublayer and circuitry dependent degenerative expression profiles in aged female Down syndrome mice. *J. Alzheimers Dis.* 100, S341–S362. doi: 10.3233/JAD-240622

Alldred, M. J., Pidikiti, H., Ibrahim, K. W., Lee, S. H., Heguy, A., Hoffman, G. E., et al. (2024b). Analysis of microisolated frontal cortex excitatory layer III and V pyramidal neurons reveals a neurodegenerative phenotype in individuals with Down syndrome. *Acta Neuropathol.* 148:16. doi: 10.1007/s00401-024-02768-0

Al-Onaizi, M. A., Parfitt, G. M., Kolisnyk, B., Law, C. S., Guzman, M. S., Barros, D. M., et al. (2017). Regulation of cognitive processing by hippocampal cholinergic tone. *Cereb. Cortex* 27, 1615–1628. doi: 10.1093/cercor/bhv349

Altafaj, X., Martin, E. D., Ortiz-Abalia, J., Valderrama, A., Lao-Peregrin, C., Dierssen, M., et al. (2013). Normalization of Dyrk1A expression by AAV2/1-shDyrk1A attenuates hippocampal-dependent defects in the Ts65Dn mouse model of Down syndrome. *Neurobiol. Dis.* 52, 117–127. doi: 10.1016/j.nbd.2012.11.017

Andrews, S. (2010). FastQC: A quality control tool for high throughput sequence data. Available at: https://www.bioinformatics.babraham.ac.uk//projects/fastqc/

Ash, J. A., Velazquez, R., Kelley, C. M., Powers, B. E., Ginsberg, S. D., Mufson, E. J., et al. (2014). Maternal choline supplementation improves spatial mapping and increases basal forebrain cholinergic neuron number and size in aged Ts65Dn mice. *Neurobiol. Dis.* 70, 32–42. doi: 10.1016/j.nbd.2014.06.001

Ashburner, M., Ball, C. A., Blake, J. A., Botstein, D., Butler, H., Cherry, J. M., et al. (2000). Gene ontology: tool for the unification of biology. The Gene Ontology Consortium. *Nat Genet* 25, 25–29. doi: 10.1038/75556

Bayona-Bafaluy, M. P., Garrido-Perez, N., Meade, P., Iglesias, E., Jimenez-Salvador, I., Montoya, J., et al. (2021). Down syndrome is an oxidative phosphorylation disorder. *Redox Biol.* 41:101871. doi: 10.1016/j.redox.2021.101871

Belichenko, P. V., Kleschevnikov, A. M., Salehi, A., Epstein, C. J., and Mobley, W. C. (2007). Synaptic and cognitive abnormalities in mouse models of Down syndrome: exploring genotype-phenotype relationships. *J. Comp. Neurol.* 504, 329–345. doi: 10.1002/cne.21433

Belichenko, P. V., Masliah, E., Kleschevnikov, A. M., Villar, A. J., Epstein, C. J., Salehi, A., et al. (2004). Synaptic structural abnormalities in the Ts65Dn mouse model of Down syndrome. *J. Comp. Neurol.* 480, 281–298. doi: 10.1002/cne.20337

Bianchi, P., Ciani, E., Guidi, S., Trazzi, S., Felice, D., Grossi, G., et al. (2010). Early pharmacotherapy restores neurogenesis and cognitive performance in the Ts65Dn mouse model for Down syndrome. *J. Neurosci.* 30, 8769–8779. doi: 10.1523/JNEUROSCI.0534-10.2010

Bofill-De Ros, X., Santos, M., Vila-Casadesus, M., Villanueva, E., Andreu, N., Dierssen, M., et al. (2015). Genome-wide miR-155 and miR-802 target gene identification in the hippocampus of Ts65Dn Down syndrome mouse model by miRNA sponges. *BMC Genomics* 16:907. doi: 10.1186/s12864-015-2160-6

Bolger, A. M., Lohse, M., and Usadel, B. (2014). Trimmomatic: a flexible trimmer for Illumina sequence data. *Bioinformatics* 30, 2114–2120. doi: 10.1093/bioinformatics/btu170

Broberg, P. (2005). A comparative review of estimates of the proportion unchanged genes and the false discovery rate. *Bmc Bioinformatics* 6:199. doi: 10.1186/1471-2105-6-199

Cataldo, A. M., Petanceska, S., Peterhoff, C. M., Terio, N. B., Epstein, C. J., Villar, A., et al. (2003). App gene dosage modulates endosomal abnormalities of Alzheimer's disease in a segmental trisomy 16 mouse model of Down syndrome. *J. Neurosci.* 23, 6788–6792. doi: 10.1523/JNEUROSCI.23-17-06788.2003

Cataldo, A. M., Peterhoff, C. M., Troncoso, J. C., Gomez-Isla, T., Hyman, B. T., and Nixon, R. A. (2000). Endocytic pathway abnormalities precede amyloid beta deposition in sporadic Alzheimer's disease and Down syndrome: differential effects of APOE genotype and presenilin mutations. *Am. J. Pathol.* 157, 277–286. doi: 10.1016/S0002-9440(10)64538-5

Chakrabarti, L., Best, T. K., Cramer, N. P., Carney, R. S., Isaac, J. T., Galdzicki, Z., et al. (2010). Olig1 and Olig2 triplication causes developmental brain defects in Down syndrome. *Nat. Neurosci.* 13, 927–934. doi: 10.1038/nn.2600

Chapman, R. S., and Hesketh, L. J. (2000). Behavioral phenotype of individuals with Down syndrome. *Ment. Retard. Dev. Disabil. Res. Rev.* 6, 84–95. doi: 10.1002/1098-2779(2000)6:2<84::AID-MRDD2>3.0.CO;2-P

Choi, J. H., Berger, J. D., Mazzella, M. J., Morales-Corraliza, J., Cataldo, A. M., Nixon, R. A., et al. (2009). Age-dependent dysregulation of brain amyloid precursor protein in the Ts65Dn Down syndrome mouse model. *J. Neurochem.* 110, 1818–1827. doi: 10.1111/j.1471-4159.2009.06277.x

Contestabile, A., Greco, B., Ghezzi, D., Tucci, V., Benfenati, F., and Gasparini, L. (2013). Lithium rescues synaptic plasticity and memory in Down syndrome mice. *J. Clin. Invest.* 123, 348–361. doi: 10.1172/JCI64650

Contestabile, A., Magara, S., and Cancedda, L. (2017). The Gabaergic hypothesis for cognitive disabilities in Down syndrome. *Front. Cell. Neurosci.* 11:54. doi: 10.3389/fncel.2017.00054

Costa, A. C. (2011). On the promise of pharmacotherapies targeted at cognitive and neurodegenerative components of Down syndrome. *Dev. Neurosci.* 33, 414–427. doi: 10.1159/000330861

Costa, A. C., and Grybko, M. J. (2005). Deficits in hippocampal CA1 LTP induced by TBS but not HFS in the Ts65Dn mouse: a model of Down syndrome. *Neurosci. Lett.* 382, 317–322. doi: 10.1016/j.neulet.2005.03.031

Costa, A. C., Scott-Mckean, J. J., and Stasko, M. R. (2008). Acute injections of the NMDA receptor antagonist memantine rescue performance deficits of the Ts65Dn mouse model of Down syndrome on a fear conditioning test. *Neuropsychopharmacology* 33, 1624–1632. doi: 10.1038/sj.npp.1301535

Das, D., Phillips, C., Hsieh, W., Sumanth, K., Dang, V., and Salehi, A. (2014). Neurotransmitter-based strategies for the treatment of cognitive dysfunction in Down syndrome. *Prog. Neuro-Psychopharmacol. Biol. Psychiatry* 54, 140–148. doi: 10.1016/j.pnpbp.2014.05.004

Davisson, M. T., Schmidt, C., Reeves, R. H., Irving, N. G., Akeson, E. C., Harris, B. S., et al. (1993). Segmental trisomy as a mouse model for Down syndrome. *Prog. Clin. Biol. Res.* 384, 117–133.

Digma, L. A., Winer, J. R., and Greicius, M. D. (2024). Substantial doubt remains about the efficacy of anti-amyloid antibodies. *J. Alzheimers Dis.* 97, 567–572. doi: 10.3233/JAD-231198

Dobin, A., Davis, C. A., Schlesinger, F., Drenkow, J., Zaleski, C., Jha, S., et al. (2013). Star: ultrafast universal RNA-seq aligner. *Bioinformatics* 29, 15–21. doi: 10.1093/bioinformatics/bts635

Dowjat, W. K., Adayev, T., Kuchna, I., Nowicki, K., Palminiello, S., Hwang, Y. W., et al. (2007). Trisomy-driven overexpression of DYRK1A kinase in the brain of subjects with Down syndrome. *Neurosci. Lett.* 413, 77–81. doi: 10.1016/j.neulet.2006.11.026

Duchon, A., Raveau, M., Chevalier, C., Nalesso, V., Sharp, A. J., and Herault, Y. (2011). Identification of the translocation breakpoints in the Ts65Dn and Ts1Cje mouse lines: relevance for modeling Down syndrome. *Mamm. Genome* 22, 674–684. doi: 10.1007/s00335-011-9356-0

Ebell, M. H., Barry, H. C., Baduni, K., and Grasso, G. (2024). Clinically important benefits and harms of monoclonal antibodies targeting amyloid for the treatment of Alzheimer disease: a systematic review and meta-analysis. *Ann. Fam. Med.* 22, 50–62. doi: 10.1370/afm.3050

Emili, M., Stagni, F., Bonasoni, M. P., Guidi, S., and Bartesaghi, R. (2024). Cellularity defects are not ubiquitous in the brains of fetuses with Down syndrome. *Dev. Neurobiol.* 84, 264–273. doi: 10.1002/dneu.22953

Feki, A., and Hibaoui, Y. (2018). Dyrk1A ProteinA promising therapeutic target to improve cognitive deficits in Down Syndrome. *Brain Sci.* 8. doi: 10.3390/brainsci8100187

Fernandez, F., and Garner, C. C. (2008). Episodic-like memory in Ts65Dn, a mouse model of Down syndrome. *Behav. Brain Res.* 188, 233–237. doi: 10.1016/j.bbr.2007.09.015

Fernandez, F., Morishita, W., Zuniga, E., Nguyen, J., Blank, M., Malenka, R. C., et al. (2007). Pharmacotherapy for cognitive impairment in a mouse model of Down syndrome. *Nat. Neurosci.* 10, 411–413. doi: 10.1038/nn1860

Fernández-Cabello, S., Kronbichler, M., Van Dijk, K. R. A., Goodman, J. A., Spreng, R. N., and Schmitz, T. W. (2020). Basal forebrain volume reliably predicts the cortical spread of Alzheimer's degeneration. *Brain* 143, 993–1009. doi: 10.1093/brain/awaa012

Filzmoser, P., and Todorov, V. (2013). Robust tools for the imperfect world. *Inf. Sci.* 245, 4–20. doi: 10.1016/j.ins.2012.10.017

Freeburn, A., and Munn, R. G. K. (2021). Signalling pathways contributing to learning and memory deficits in the Ts65Dn mouse model of Down syndrome. *Neuronal Signaling* 5:NS20200011. doi: 10.1042/NS20200011

Gautier, M. K., Kelley, C. M., Lee, S. H., Alldred, M. J., Mcdaid, J., Mufson, E. J., et al. (2023). Maternal choline supplementation protects against age-associated cholinergic and Gabaergic basal forebrain neuron degeneration in the Ts65Dn mouse model of Down syndrome and Alzheimer's disease. *Neurobiol. Dis.* 188:106332. doi: 10.1016/j.nbd.2023.106332

Gene Ontology Consortium (2021). The gene ontology resource: enriching a gold mine. *Nucleic Acids Res.* 49, D325–d334. doi: 10.1093/nar/gkaa1113

Ginsberg, S. D. (2010). Alterations in discrete glutamate receptor subunits in adult mouse dentate gyrus granule cells following perforant path transection. *Anal. Bioanal. Chem.* 397, 3349–3358. doi: 10.1007/s00216-010-3826-1

Ginsberg, S. D., Che, S., Wuu, J., Counts, S. E., and Mufson, E. J. (2006). Down regulation of TRK but not p75NTR gene expression in single cholinergic basal forebrain neurons mark the progression of Alzheimer's disease. *J. Neurochem.* 97, 475–487. doi: 10.1111/j.1471-4159.2006.03764.x

Gotti, S., Caricati, E., and Panzica, G. (2011). Alterations of brain circuits in Down syndrome murine models. *J. Chem. Neuroanat.* 42, 317–326. doi: 10.1016/j.jchemneu.2011.09.002

Granholm, A. C., Sanders, L. A., and Crnic, L. S. (2000). Loss of cholinergic phenotype in basal forebrain coincides with cognitive decline in a mouse model of Down's syndrome. *Exp. Neurol.* 161, 647–663. doi: 10.1006/exnr.1999.7289

Granholm, A. C., Sanders, L., Seo, H., Lin, L., Ford, K., and Isacson, O. (2003). Estrogen alters amyloid precursor protein as well as dendritic and cholinergic markers in a mouse model of Down syndrome. *Hippocampus* 13, 905–914. doi: 10.1002/hipo.10130

Granno, S., Nixon-Abell, J., Berwick, D. C., Tosh, J., Heaton, G., Almudimeegh, S., et al. (2019). Downregulated Wnt/β-catenin signalling in the Down syndrome hippocampus. *Sci. Rep.* 9:7322. doi: 10.1038/s41598-019-43820-4

Hamlett, E. D., Boger, H. A., Ledreux, A., Kelley, C. M., Mufson, E. J., Falangola, M. F., et al. (2016). Cognitive impairment, neuroimaging, and Alzheimer neuropathology in mouse models of Down syndrome. *Curr. Alzheimer Res.* 13, 35–52. doi: 10.2174/1567205012666150921095505

Hanson, J. E., Blank, M., Valenzuela, R. A., Garner, C. C., and Madison, D. V. (2007). The functional nature of synaptic circuitry is altered in area CA3 of the hippocampus in a mouse model of Down's syndrome. *J. Physiol.* 579, 53–67. doi: 10.1113/jphysiol.2006.114868

Heberle, H., Meirelles, G. V., Da Silva, F. R., Telles, G. P., and Minghim, R. (2015). InteractiVenn: a web-based tool for the analysis of sets through Venn diagrams. *BMC Bioinformatics* 16:169. doi: 10.1186/s12859-015-0611-3

Hoffman, G. E., and Roussos, P. (2021). Dream: powerful differential expression analysis for repeated measures designs. *Bioinformatics* 37, 192–201. doi: 10.1093/bioinformatics/btaa687

Hoffman, G. E., and Schadt, E. E. (2016). variancePartition: interpreting drivers of variation in complex gene expression studies. *BMC Bioinformatics* 17:483. doi: 10.1186/s12859-016-1323-z

Holtzman, D. M., Santucci, D., Kilbridge, J., Chua-Couzens, J., Fontana, D. J., Daniels, S. E., et al. (1996). Developmental abnormalities and age-related neurodegeneration in a mouse model of Down syndrome. *Proc. Natl. Acad. Sci. USA* 93, 13333–13338. doi: 10.1073/pnas.93.23.13333

Hu, Y., Liu, F., Peng, W., Song, S., Zhang, C., and Meng, X. (2022). Overexpression of miR-99a in hippocampus leads to impairment of reversal learning in mice. *Behav. Brain Res.* 416:113542. doi: 10.1016/j.bbr.2021.113542

Hunter, C. L., Bimonte, H. A., and Granholm, A.-C. E. (2003a). Behavioral comparison of 4 and 6 month-old Ts65Dn mice: age-related impairments in working and reference memory. *Behav. Brain Res.* 138, 121–131. doi: 10.1016/S0166-4328(02)00275-9

Hunter, C. L., Isacson, O., Nelson, M., Bimonte-Nelson, H., Seo, H., Lin, L., et al. (2003b). Regional alterations in amyloid precursor protein and nerve growth factor across age in a mouse model of Down's syndrome. *Neurosci. Res.* 45, 437–445. doi: 10.1016/S0168-0102(03)00005-1

Hyde, L. A., and Crnic, L. S. (2001). Age-related deficits in context discrimination learning in Ts65Dn mice that model Down syndrome and Alzheimer's disease. *Behav. Neurosci.* 115, 1239–1246. doi: 10.1037/0735-7044.115.6.1239

Insausti, A. M., Megias, M., Crespo, D., Cruz-Orive, L. M., Dierssen, M., Vallina, I. F., et al. (1998). Hippocampal volume and neuronal number in Ts65Dn mice: a murine model of Down syndrome. *Neurosci. Lett.* 253, 175–178. doi: 10.1016/S0304-3940(98)00641-7

Kang, X., Wang, D., Zhang, L., Huang, T., Liu, S., Feng, X., et al. (2023). Exendin-4 ameliorates tau hyperphosphorylation and cognitive impairment in type 2 diabetes through acting on Wnt/β-catenin/NeuroD1 pathway. *Mol. Med.* 29:118. doi: 10.1186/s10020-023-00718-2

Kazuki, Y., Gao, F. J., Li, Y., Moyer, A. J., Devenney, B., Hiramatsu, K., et al. (2020). A non-mosaic transchromosomic mouse model of Down syndrome carrying the long arm of human chromosome 21. *eLife* 9:56223. doi: 10.7554/eLife.56223

Kelley, C. M., Ash, J. A., Powers, B. E., Velazquez, R., Alldred, M. J., Ikonomovic, M. D., et al. (2016). Effects of maternal choline supplementation on the septohippocampal cholinergic system in the Ts65Dn mouse model of Down syndrome. *Curr. Alzheimer Res.* 13, 84–96. doi: 10.2174/1567205012666150921100515

Kelley, C. M., Powers, B. E., Velazquez, R., Ash, J. A., Ginsberg, S. D., Strupp, B. J., et al. (2014a). Maternal choline supplementation differentially alters the basal forebrain cholinergic system of young-adult Ts65Dn and disomic mice. *J. Comp. Neurol.* 522, 1390–1410. doi: 10.1002/cne.23492

Kelley, C. M., Powers, B. E., Velazquez, R., Ash, J. A., Ginsberg, S. D., Strupp, B. J., et al. (2014b). Sex differences in the cholinergic basal forebrain in the Ts65Dn mouse model of Down syndrome and Alzheimer's disease. *Brain Pathol.* 24, 33–44. doi: 10.1111/bpa.12073

Kleschevnikov, A. M., Belichenko, P. V., Faizi, M., Jacobs, L. F., Htun, K., Shamloo, M., et al. (2012a). Deficits in cognition and synaptic plasticity in a mouse model of Down syndrome ameliorated by GABAB receptor antagonists. *J. Neurosci.* 32, 9217–9227. doi: 10.1523/JNEUROSCI.1673-12.2012

Kleschevnikov, A. M., Belichenko, P. V., Gall, J., George, L., Nosheny, R., Maloney, M. T., et al. (2012b). Increased efficiency of the GABAA and GABAB receptor-mediated neurotransmission in the Ts65Dn mouse model of Down syndrome. *Neurobiol. Dis.* 45, 683–691. doi: 10.1016/j.nbd.2011.10.009

Kleschevnikov, A. M., Belichenko, P. V., Villar, A. J., Epstein, C. J., Malenka, R. C., and Mobley, W. C. (2004). Hippocampal long-term potentiation suppressed by increased inhibition in the Ts65Dn mouse, a genetic model of Down syndrome. *J. Neurosci.* 24, 8153–8160. doi: 10.1523/JNEUROSCI.1766-04.2004

Krämer, A., Green, J., Pollard, J., and Tugendreich, S. (2013). Causal analysis approaches in ingenuity pathway analysis. *Bioinformatics* 30, 523–530. doi: 10.1093/bioinformatics/btt703

Kurt, M. A., Kafa, M. I., Dierssen, M., and Davies, D. C. (2004). Deficits of neuronal density in Ca1 and synaptic density in the dentate gyrus, CA3 and CA1, in a mouse model of Down syndrome. *Brain Res.* 1022, 101–109. doi: 10.1016/j.brainres.2004.06.075

Landes, S. D., Stevens, J. D., and Turk, M. A. (2020). Cause of death in adults with Down syndrome in the United States. *Disabil. Health J.* 13:100947. doi: 10.1016/j.dhjo.2020.100947

Li, B., and Dewey, C. N. (2011). RSEM: accurate transcript quantification from RNA-Seq data with or without a reference genome. *BMC Bioinformatics* 12:323. doi: 10.1186/1471-2105-12-323

Lind, A., Boraxbekk, C. J., Petersen, E. T., Paulson, O. B., Siebner, H. R., and Marsman, A. (2020). Regional Myo-inositol, Creatine, and choline levels are higher at older age and scale negatively with visuospatial working memory: a cross-sectional proton MR spectroscopy study at 7 tesla on Normal cognitive ageing. *J. Neurosci.* 40, 8149–8159. doi: 10.1523/JNEUROSCI.2883-19.2020

Lockrow, J., Prakasam, A., Huang, P., Bimonte-Nelson, H., Sambamurti, K., and Granholm, A. C. (2009). Cholinergic degeneration and memory loss delayed by vitamin E in a Down syndrome mouse model. *Exp. Neurol.* 216, 278–289. doi: 10.1016/j.expneurol.2008.11.021

Lott, I. T. (2012). Neurological phenotypes for Down syndrome across the life span. *Prog. Brain Res.* 197, 101–121. doi: 10.1016/B978-0-444-54299-1.00006-6

Lott, I. T., and Head, E. (2019). Dementia in Down syndrome: unique insights for Alzheimer disease research. *Nat. Rev. Neurol.* 15, 135–147. doi: 10.1038/s41582-018-0132-6

Mai, C. T., Isenburg, J. L., Canfield, M. A., Meyer, R. E., Correa, A., Alverson, C. J., et al. (2019). National population-based estimates for major birth defects, 2010-2014. *Birth Defects Res* 111, 1420–1435. doi: 10.1002/bdr2.1589

Mann, D. M., Yates, P. O., and Marcyniuk, B. (1984). Alzheimer's presenile dementia, senile dementia of Alzheimer type and Down's syndrome in middle age form an age related continuum of pathological changes. *Neuropathol. Appl. Neurobiol.* 10, 185–207. doi: 10.1111/j.1365-2990.1984.tb00351.x

Mathews, P. M., Jiang, Y., Schmidt, S. D., Grbovic, O. M., Mercken, M., and Nixon, R. A. (2002). Calpain activity regulates the cell surface distribution of amyloid precursor protein. Inhibition of clapains enhances endosomal generation of beta-cleaved C-terminal APP fragments. *J. Biol. Chem.* 277, 36415–36424. doi: 10.1074/jbc.M205208200

Mathys, H., Peng, Z., Boix, C. A., Victor, M. B., Leary, N., Babu, S., et al. (2023). Single-cell atlas reveals correlates of high cognitive function, dementia, and resilience to Alzheimer's disease pathology. *Cell* 186, 4365–4385.e27. doi: 10.1016/j.cell.2023.08.039

Mufson, E. J., Ginsberg, S. D., Ma, T., Ledreux, A., and Perez, S. E. (2021). Editorial: Down syndrome, neurodegeneration and dementia. *Front. Aging Neurosci.* 13:791044. doi: 10.3389/fnagi.2021.791044

Mufson, E. J., Ikonomovic, M. D., Counts, S. E., Perez, S. E., Malek-Ahmadi, M., Scheff, S. W., et al. (2016). Molecular and cellular pathophysiology of preclinical Alzheimer's disease. *Behav. Brain Res.* 311, 54–69. doi: 10.1016/j.bbr.2016.05.030

Omar, M. H., and Scott, J. D. (2020). AKAP Signaling Islands: venues for precision pharmacology. *Trends Pharmacol. Sci.* 41, 933–946. doi: 10.1016/j.tips.2020.09.007

Pages, H. C. M., Falcon, S., and Li, N. (2019). AnnotationDbi: Manipulation of Sqlite-based annotations in bioconductor. doi: 10.18129/B9.bioc.AnnotationDbi

Parker, S. E., Mai, C. T., Canfield, M. A., Rickard, R., Wang, Y., Meyer, R. E., et al. (2010). Updated National Birth Prevalence estimates for selected birth defects in the United States, 2004-2006. *Birth Defects Res. A Clin. Mol. Teratol.* 88, 1008–1016. doi: 10.1002/bdra.20735

Peng, S., Garzon, D. J., Marchese, M., Klein, W., Ginsberg, S. D., Francis, B. M., et al. (2009). Decreased brain-derived neurotrophic factor depends on amyloid aggregation state in transgenic mouse models of Alzheimer's disease. *J. Neurosci.* 29, 9321–9329. doi: 10.1523/JNEUROSCI.4736-08.2009

Perez, S. E., Miguel, J. C., He, B., Malek-Ahmadi, M., Abrahamson, E. E., Ikonomovic, M. D., et al. (2019). Frontal cortex and striatal cellular and molecular pathobiology in individuals with Down syndrome with and without dementia. *Acta Neuropathol.* 137, 413–436. doi: 10.1007/s00401-019-01965-6

Perez-Cruz, C., Nolte, M. W., Van Gaalen, M. M., Rustay, N. R., Termont, A., Tanghe, A., et al. (2011). Reduced spinedensity in specific regions of CA1 pyramidal neurons in two transgenic mouse models of Alzheimer's disease. *J. Neurosci.* 31, 3926–3934. doi: 10.1523/JNEUROSCI.6142-10.2011

Picard Toolkit. (2019). Picard toolkit [online]. Broad Institute, Github Repository. Available online at: https://broadinstitute.github.io/picard/ (Accessed August 24, 22)

Pollonini, G., Gao, V., Rabe, A., Palminiello, S., Albertini, G., and Alberini, C. M. (2008). Abnormal expression of synaptic proteins and neurotrophin-3 in the Down syndrome mouse model Ts65Dn. *Neuroscience* 156, 99–106. doi: 10.1016/j.neuroscience.2008.07.025

Popov, V. I., Kleschevnikov, A. M., Klimenko, O. A., Stewart, M. G., and Belichenko, P. V. (2011). Three-dimensional synaptic ultrastructure in the dentate gyrus and hippocampal area CA3 in the Ts65Dn mouse model of Down syndrome. *J. Comp. Neurol.* 519, 1338–1354. doi: 10.1002/cne.22573

Powers, B. E., Velazquez, R., Kelley, C. M., Ash, J. A., Strawderman, M. S., Alldred, M. J., et al. (2016). Attentional function and basal forebrain cholinergic neuron morphology during aging in the Ts65Dn mouse model of Down syndrome. *Brain Struct. Funct.* 221, 4337–4352. doi: 10.1007/s00429-015-1164-y

Qiagen. (2020). Qiagen bioinformatics. Available online at: https://www.qiagenbioinformatics.com/products/ingenuity-pathway-analysis

Rachidi, M., and Lopes, C. (2008). Mental retardation and associated neurological dysfunctions in Down syndrome: a consequence of dysregulation in critical chromosome 21 genes and associated molecular pathways. *Eur. J. Paediatr. Neurol.* 12, 168–182. doi: 10.1016/j.ejpn.2007.08.010

Rau, A., Gallopin, M., Celeux, G., and Jaffrézic, F. (2013). Data-based filtering for replicated high-throughput transcriptome sequencing experiments. *Bioinformatics* 29, 2146–2152. doi: 10.1093/bioinformatics/btt350

Reeves, R. H., Irving, N. G., Moran, T. H., Wohn, A., Kitt, C., Sisodia, S. S., et al. (1995). A mouse model for Down syndrome exhibits learning and behaviour deficits. *Nat. Genet.* 11, 177–184. doi: 10.1038/ng1095-177

Robinson, M. D., Mccarthy, D. J., and Smyth, G. K. (2010). edgeR: a Bioconductor package for differential expression analysis of digital gene expression data. *Bioinformatics* 26, 139–140. doi: 10.1093/bioinformatics/btp616

Rueda, N., Florez, J., and Martinez-Cue, C. (2012). Mouse models of Down syndrome as a tool to unravel the causes of mental disabilities. *Neural Plast.* 2012:584071. doi: 10.1155/2012/584071

Shannon, P., Markiel, A., Ozier, O., Baliga, N. S., Wang, J. T., Ramage, D., et al. (2003). Cytoscape: a software environment for integrated models of biomolecular interaction networks. *Genome Res.* 13, 2498–2504. doi: 10.1101/gr.1239303

Shao, L. R., Gao, F., Chinnasamy, V., Kazuki, Y., Oshimura, M., Reeves, R. H., et al. (2023). Increased propensity for infantile spasms and altered neocortical excitation-inhibition balance in a mouse model of Down syndrome carrying human chromosome 21. *Neurobiol. Dis.* 184:106198. doi: 10.1016/j.nbd.2023.106198

Siarey, R. J., Carlson, E. J., Epstein, C. J., Balbo, A., Rapoport, S. I., and Galdzicki, Z. (1999). Increased synaptic depression in the Ts65Dn mouse, a model for mental retardation in Down syndrome. *Neuropharmacology* 38, 1917–1920. doi: 10.1016/S0028-3908(99)00083-0

Siarey, R. J., Stoll, J., Rapoport, S. I., and Galdzicki, Z. (1997). Altered long-term potentiation in the young and old Ts65Dn mouse, a model for Down syndrome. *Neuropharmacology* 36, 1549–1554. doi: 10.1016/S0028-3908(97)00157-3

Sierra, C., Sabariego-Navarro, M., Fernández-Blanco, Á., Cruciani, S., Zamora-Moratalla, A., Novoa, E. M., et al. (2024). The lncrna Snhg11, a new candidate contributing to neurogenesis, plasticity, and memory deficits in Down syndrome. *Mol. Psychiatry* 29, 2117–2134. doi: 10.1038/s41380-024-02440-9

Solopova, E., Romero-Fernandez, W., Harmsen, H., Ventura-Antunes, L., Wang, E., Shostak, A., et al. (2023). Fatal iatrogenic cerebral β-amyloid-related arteritis in a woman treated with lecanemab for Alzheimer's disease. *Nat. Commun.* 14:8220. doi: 10.1038/s41467-023-43933-5

Stagni, F., Magistretti, J., Guidi, S., Ciani, E., Mangano, C., Calzà, L., et al. (2013). Pharmacotherapy with fluoxetine restores functional connectivity from the dentate gyrus to field Ca3 in the Ts65Dn mouse model of Down syndrome. *PLoS One* 8:e61689. doi: 10.1371/journal.pone.0061689

Strupp, B. J., Powers, B. E., Velazquez, R., Ash, J. A., Kelley, C. M., Alldred, M. J., et al. (2016). Maternal choline supplementation: a potential prenatal treatment for Down syndrome and Alzheimer's disease. *Curr. Alzheimer Res.* 13, 97–106. doi: 10.2174/1567205012666150921100311

Sturgeon, X., and Gardiner, K. J. (2011). Transcript catalogs of human chromosome 21 and orthologous chimpanzee and mouse regions. *Mamm. Genome* 22, 261–271. doi: 10.1007/s00335-011-9321-y

Szklarczyk, D., Gable, A. L., Lyon, D., Junge, A., Wyder, S., Huerta-Cepas, J., et al. (2018). String v11: protein–protein association networks with increased coverage, supporting functional discovery in genome-wide experimental datasets. *Nucleic Acids Res.* 47, D607–D613. doi: 10.1093/nar/gky1131

Todorov, V. (2024). rrcov: scalable robust estimators with high breakdown point. Available online at: https://Cran.R-project.org/package=rrcov:Cran (Accessed January 21, 2025)

Velazquez, R., Ash, J. A., Powers, B. E., Kelley, C. M., Strawderman, M., Luscher, Z. I., et al. (2013). Maternal choline supplementation improves spatial learning and adult hippocampal neurogenesis in the Ts65Dn mouse model of Down syndrome. *Neurobiol. Dis.* 58, 92–101. doi: 10.1016/j.nbd.2013.04.016

Wang, L., Wang, S., and Li, W. (2012). RSeQC: quality control of RNA-seq experiments. *Bioinformatics* 28, 2184–2185. doi: 10.1093/bioinformatics/bts356

Wegiel, J., Kuchna, I., Nowicki, K., Frackowiak, J., Dowjat, K., Silverman, W. P., et al. (2004). Cell type-and brain structure-specific patterns of distribution of minibrain kinase in human brain. *Brain Res.* 1010, 69–80. doi: 10.1016/j.brainres.2004.03.008

Whitehouse, P. J., Price, D. L., Struble, R. G., Clark, A. W., Coyle, J. T., and Delong, M. R. (1982). Alzheimer's disease and senile dementia: loss of neurons in the basal forebrain. *Science* 215, 1237–1239. doi: 10.1126/science.7058341

Wisniewski, K. E. (1990). Down syndrome children often have brain with maturation delay, retardation of growth, and cortical dysgenesis. *Am. J. Med. Genet. Suppl.* 7, 274–281

Wisniewski, K. E., Dalton, A. J., Crapper Mclachlan, D. R., Wen, G. Y., and Wisniewski, H. M. (1985). Alzheimer's disease in Down's syndrome: clinicopathologic studies. *Neurology* 35, 957–961. doi: 10.1212/WNL.35.7.957

Yates, C. M., Simpson, J., Maloney, A. F., Gordon, A., and Reid, A. H. (1980). Alzheimer-like cholinergic deficiency in Down syndrome. *Lancet* 2:979. doi: 10.1016/s0140

Zehetmayer, S., Posch, M., and Graf, A. (2022). Impact of adaptive filtering on power and false discovery rate in RNA-seq experiments. *BMC Bioinformatics* 23:388. doi: 10.1186/s12859-022-04928-z

Zhao, J., O'connor, T., and Vassar, R. (2011). The contribution of activated astrocytes to Aβ production: implications for Alzheimer's disease pathogenesis. *J. Neuroinflammation* 8:150. doi: 10.1186/1742-2094-8-150

Zhou, Z., Zhi, C., Chen, D., Cai, Z., and Jiang, X. (2023). Single-nucleus RNA sequencing reveals cell type-specific transcriptome alterations of Down syndrome hippocampus using the Dp16 mouse model. *Genes Genomics* 45, 1305–1315. doi: 10.1007/s13258-023-01433-2

Glossary

2N - Normal disomic controls

A*β* - Amyloid-beta peptide

AD - Alzheimer's disease

APP - Amyloid precursor protein

***β*-TUBIII** - β-tubulin III

BFCNs - Basal forebrain cholinergic neurons

DEGs - Differentially expressed genes

D/Fs - Disease and functions

DGCs - Dentate gyrus granule cells

DS - Down syndrome

DYRK1A - Dual specificity tyrosine phosphorylation regulated kinase 1a.

Gnas - Guanine nucleotide binding protein, alpha stimulating

GO - Gene Ontology

HSA21 - Human chromosome 21

IPA - Ingenuity Pathway Analysis

LCM - Laser capture microdissection

LFC - Log-fold change

LTP - Long-term potentiation

MDS - Multidimensional Scaling

Mmu16 - Mouse chromosome 16

Mmu17 - Mouse chromosome 17

MO - Months of age

Pcp4 - Purkinje cell protein 4

PN - Pyramidal neuron

PPI - Protein–protein interaction

Prkar1b - Protein kinase cAMP-dependent type I regulatory subunit beta

Prkar2b - Protein kinase cAMP-dependent type II regulatory subunit beta

QC - Quality control

RIN - RNA Integrity Number

RNA-seq - RNA-sequencing

Rpl12 - Ribosomal protein L12

RT - Room temperature

THB - Tissue homogenization buffer

UMAP - UNIFORM Manifold Approximation and Projection